

Review

Nanomaterial-Based Sensors for Exhaled Breath Analysis: A Review

Mohan Velumani ^{1,†}, Asokan Prasanth ^{1,†}, Subramaniyam Narasimman ^{1,2,†}, Arunkumar Chandrasekhar ¹ , Abraham Sampson ¹, Samir Ranjan Meher ³, Sivacoumar Rajalingam ¹ , Elizabeth Rufus ^{1,*} and Zachariah C. Alex ^{1,*}

¹ School of Electronics Engineering, Vellore Institute of Technology, Vellore 632014, India

² Department of Electronics and Communication Engineering, Sri Venkateswara College of Engineering and Technology (Autonomous), Chittoor 517127, India

³ Department of Physics, School of Advanced Sciences, Vellore Institute of Technology, Vellore 632014, India

* Correspondence: elizabethrufus@vit.ac.in (E.R.); zachariahalex@vit.ac.in (Z.C.A.)

† These authors contributed equally to this work.

Abstract: The quantification of gases in breath has gained significant attention as a modern diagnosis method due to its non-invasive nature, and as a painless and straightforward method for the early detection of physiological disorders. Several notable clinical applications have been established for disease diagnosis by correlating exhaled breath samples and specific diseases. In addition, diverse breath molecules represent a biomarker of specific illnesses and are precisely identified by the standard analytical method. However, because of the bulky equipment size, expensive cost, and complexity in measurement when using analytical methods, many researchers are focusing on developing highly selective, sensitive, stable, robust, and economical sensors for breath analysis. It is essential to optimize approaches such as breath sampling, biomarker sensing, data analysis, etc. However, the detection of ppb-level biomarkers in exhaled breath is too challenging to solve due to the abundance of interfering gases. We present a brief and comprehensive review of a recent diagnostic technique that employs nanomaterial (NM)-based sensors to identify the volatile organic compounds (VOCs) associated to diseases. Because they are easily fabricated, chemically versatile, and can be integrated with existing sensing platforms, NMs are ideal for such sensors. Initially, this review provides crucial details about certain representative biomarkers found in diseased patients' exhaled breath and the demand for breath sensors. Subsequently, the review highlights diverse sensor technologies such as electrical, optical, and mass-sensitive gas sensors and describes their sensing capability for detecting the biomarkers' concentrations and their primary endeavor of diagnosing disease. Finally, the pitfalls and challenges of sensor characteristics are discussed. This article lays the basis for developing high-performance gas sensors based on novel NMs.



Citation: Velumani, M.; Prasanth, A.; Narasimman, S.; Chandrasekhar, A.; Sampson, A.; Meher, S.R.; Rajalingam, S.; Rufus, E.; Alex, Z.C. Nanomaterial-Based Sensors for Exhaled Breath Analysis: A Review. *Coatings* **2022**, *12*, 1989. <https://doi.org/10.3390/coatings12121989>

Academic Editor: Hyung-Ho Park

Received: 12 November 2022

Accepted: 12 December 2022

Published: 19 December 2022

Publisher's Note: MDPI stays neutral with regard to jurisdictional claims in published maps and institutional affiliations.



Copyright: © 2022 by the authors. Licensee MDPI, Basel, Switzerland. This article is an open access article distributed under the terms and conditions of the Creative Commons Attribution (CC BY) license (<https://creativecommons.org/licenses/by/4.0/>).

1. Introduction

Volatile organic compounds' (VOCs') detection in exhaled breath is a modern diagnostic technique, and is a rapid, selective, point of care, and non-invasive approach for the diagnosis of various human diseases. Recently, VOC-based diagnostic technologies have attracted significant attention worldwide. They enable instantaneous monitoring of high-risk populations, together with early diagnosis and the effectiveness of therapy. Most importantly, VOCs are produced in the human body by altering metabolic pathways related to carbohydrate metabolism, liver enzymes, lipid metabolism, oxidative stress, and cytochrome P450 [1,2]. This exhaled breath concentration could be a reliable and precious indicator of human health condition.

In the 1990s, breath analysis towards identifying biomarkers for specific diseases and its detection methods became a significant research focus in the biomedical domain [3].

Nearly 1000 VOCs are reported to exist in exhaled human breath corresponding to several chronic diseases, including diabetes, cancers, chronic kidney diseases, tuberculosis, and cognitive diseases [4–6]. However, breath analysis for disease diagnosis is insubstantial because of non-reliable optimization and there being fewer datasets.

In prior reports, numerous variabilities in the diagnostic utility of exhaled breath analysis were addressed [7,8]. Nevertheless, the distinguishable breath VOCs and their concentration (parts per million (ppm) to sub-ppm level) are different in sick humans from those of healthy humans. The exhaled breath analysis schematic diagram is shown in Figure 1 [9]. The detection of various VOC biomarkers from exhaled breath can be the fingerprint for the early detection of health risks and the diagnosis of several chronic diseases. The VOC biomarkers can be detected using conventional diagnosis tools such as the Fourier transform infrared spectrometer (FTIR), gas chromatography–mass spectrometer (GC-MS), non-dispersive infrared spectroscopy (NDIR), chemiluminescence, surface acoustic wave (SAW), electrochemical, colorimetric, and selected ion flow tube (SIFT) methods [10]. Although the techniques above exhibit rapid and high selectivity of target VOCs, they have complexities such as size, cost, the need for proficient personnel, and time-consuming processes [11]. These limitations can be overcome with NM-based exhaled breath sensors because of their potential for building real-time, low-cost, and easily fabricated systems [12]. In the last decade, NM-based sensors have attracted tremendous interest in breath testing because of their fast response time (<10 s), limit of detection (LOD), and cost-effectiveness compared with other existing techniques such as GC-MS, biopsy, and other imaging techniques [13]. NMs have advantages such as a high surface-to-volume ratio, nanometer-sized materials, and outstanding electronic (or ionic) charge-carrying characteristics [14,15]. In addition, NMs can be readily fabricated or incorporated into devices to develop upgraded sensing platforms. A set of such inherent characteristics has resulted in many applications of NMs in numerous fields of science and technology.

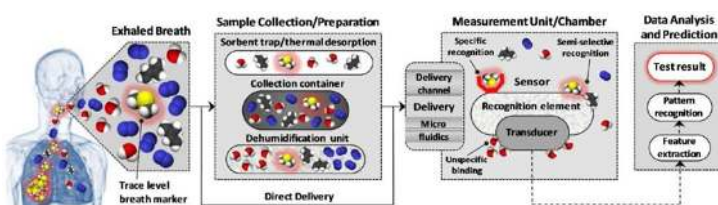


Figure 1. Schematic of various steps followed for analysis of exhaled breath. Reprinted with permission from Ref. [9] Copyright 2014 American Chemical Society.

This comprehensive review systematically discusses various exhaled breath biomarkers, conventional analytical devices, and their detection techniques. Primarily, we summarize several aspects of exhaled breath sensors, such as material composition, structure, and morphology. Then, we discuss the recent developments in NM-based devices (optical, electrical, and quartz crystal microbalance and Field Effect Transistor (FET)), involving carbon nanotubes, metal oxide semiconductors, and polymers as the sensing materials. The literature reported within the present review shows that the most optimistic NM-based sensors can deliver modest sensitivity and specificity. Further, technological challenges and future research endeavors are discussed in depth during this research field.

2. Origin of Biomarkers for Exhaled Breath Analysis

Thousands of VOCs are observed in the exhaled breath of humans [16]. The volatile compounds represent the biochemical activity state of cells and tissues and indicate the blueprint of human health. These VOCs are typically from three origins, which are explained below.

The first is the direct metabolic activity in airway tissue relevant to pulmonary diseases. Compared with the genetic methods, changes in the concentration of the metabolites are due to a change in the single gene, resulting in the emission of hundreds of different volatile compounds. It is not detectable in blood-based testing. Next, VOC biomarkers relevant to the early stages of malignant/non-malignant diseases and non-pulmonary diseases were identified as exchanging chemicals with the blood circulatory system. The human circulatory system takes around a minute to circulate the blood in the entire body. The exhaled breath sampling for the same period continuously reveals the details of the body's health condition non-invasively. Even the blood sampling-based disease diagnosis would not reveal much lower concentrations of the chemicals present, but the sensitivity will be less in the non-invasive technique. Third, the external environment may present exogenous molecules such as microbes and other VOCs in exhaled breath.

In addition to the biochemical pathways of the biomarkers, it is necessary to analyze how these biomarkers are produced. The exhaled breath biomarker contains various VOCs, including hydrocarbons, oxygen, and sulfur-containing compounds. Among them, acetone, ethanol, methanol, and other alcohols have been identified as some of the key VOC components in estimating the disease states in human beings. Knowing these VOCs are generated in the human body and are related to the diseased condition is essential. For example, the release of acetone in human breath is due to acetoacetate decarboxylation. Methanol and ethanol originate in the gastrointestinal tract due to microbe fermentation of carbohydrates. Likewise, lipid peroxidation in the human body produces ethane and pentanes. The incomplete metabolism of methionine results in the production of sulfur compounds. The release of ammonia in the breath is the byproduct of protein breakdown. By understanding these biomarkers and their respective origins, exhaled breath analysis can play a significant role in the non-invasive diagnosis. [17]. The summary of the main VOCs from some non-communicable diseases is listed below in Table 1.

Table 1. Summary of main VOCs from selected non-communicable diseases.

No.	Disease	Disease-Related VOCs	Sample Sources	Ref.
1	Diabetes	Acetone; methyl nitrate; ethanol; Octane; pentane; decane; 2-methylpentane; heptane; 2,3,5-trimethylhexane; 2,4-dimethyl-1-heptane;	Breath	Novak et al., Galassetti et al. [18,19]
2	Lung Cancer	4-methyloctane; isoprene; benzene; 1-propanol; acetone; butyl acetate; 2-pentane; toluene; styrene; 2,3,3-trimethylpentane; 2,4-dimethyl-1-heptane; 3,3-dimethylpentane; 5-(2-methylpropyl)nonane;	Breath; blood; urine.	Hakim et al. [20]
3	Breast Cancer	2-amino-5-isopropyl-8-methyl-1-azulenecarbonitrile; 2,3,4-trimethyldecane;	Breath	Zhang et al., Phillips et al. [21,22]
4	Halitosis	Hydrogen sulphide; methanethiol	Breath	Choi et al. [23]
5	Kidney diseases	Ammonia	Breath	Spanel et al., Obermeier et al. [24,25]

3. Various Detection Techniques for Exhaled Breath VOCs

Over the last five decades, several detection techniques have been utilized for VOC sensing. These detection techniques are classified into physical and chemical methods. Table 2 discusses the various detection principles. In the physical methods, various spectroscopic techniques are widely used in exhaled breath VOC analysis. Among them, proton-transfer-reaction mass spectrometry (PTR-MS), gas chromatography–mass spectroscopy (GS-MS), ion mobility spectrometry, and selected ion flow tube technique mass spectrometry (SIFT-MS) are used to detect lower concentrations of VOCs [26–35]. Similarly, various chemical methods such as electrical, optical, acoustic, calorimetric, and electrochemical sensors have been widely used [36–40]. Utilizing these chemical methods, various nanomaterials have been reported as the sensing layer for VOC sensing. Along with the abovementioned sensing principles, researchers have focused on materials and fabrication techniques to achieve better sensor response characteristics.

Table 2. Various detection techniques for exhaled breath VOCs.

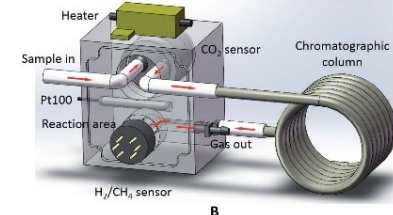
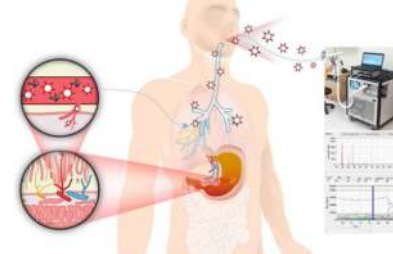
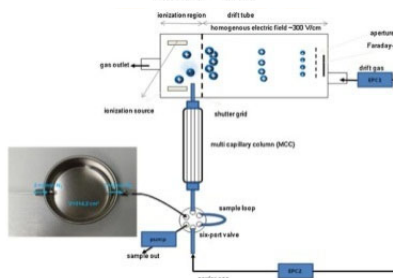
Detection Methods	Principle	Advantages	Disadvantages	Image	References
Physical Methods					
1. Physical Spectroscopic Techniques					
1.1. Mass Spectroscopy					
GC-MS	Analytes were separated and detected using ionization method	High sensitivity; high selectivity	Bulky; expensive; time-consuming		F. Gao et al. Reprinted with permission from Ref. [41] Copyright 2009 RSC Publishing
PTR-MS	Volatile compounds are ionized using gas phase H3O+ ions, which are subsequently separated using a mass spectrometer based on their m/z ratio	High sensitivity and the possibility of rapid quantification	Proton affinity greater than water molecule can only be detected		Y. Jung et al. [42]
SIFT-IMS	The mobility of each ion based on the applied electric field is related to the velocity of the ion	Eliminate need for sample preparation and pre-quantification, real-time measurements	Identification of VOCs are not always possible, no extensive compound library exists as with GC-MS		V. Ruzsanyi et al. Reprinted with permission from Ref. [43] Copyright 2012 Elsevier

Table 2. *Cont.*

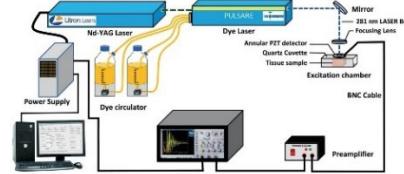
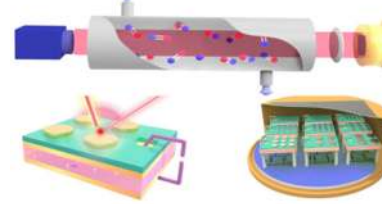
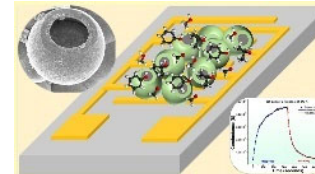
Detection Methods	Principle	Advantages	Disadvantages	Image	References
1.2. Laser Spectroscopy					
PAS	Quantity of light absorbed by a gas molecule or free atoms at a certain wavelength	Very sensitive, easy, efficient, and robust analytical method	Cost of the equipment.		J. Rodrigues et al. [44]
MID-IR	Measurement of intensity variation in functional groups	Ultra trace sensitivity, high spectral resolution, non-destructive, label-free	Beam divergence		X. Tan et al. [45]
Chemical Methods					
1. Nanomaterial-based techniques					
1.1. Electrical					
Chemiresistors	Change in resistance or conductivity	Low cost; short response time, long-lasting	Relatively low sensitivity; high energy consumption		S. Acharyya et al. Reprinted with permission from Ref. [46] Copyright 2021 American Chemical Society

Table 2. Cont.

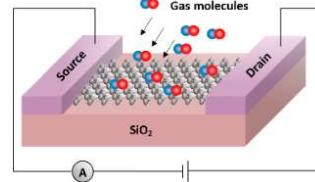
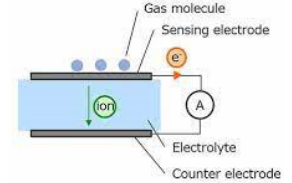
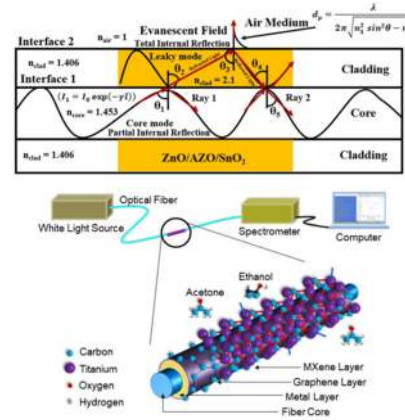
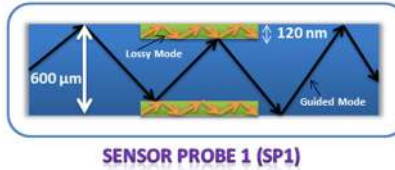
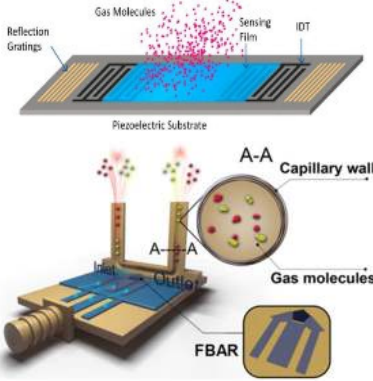
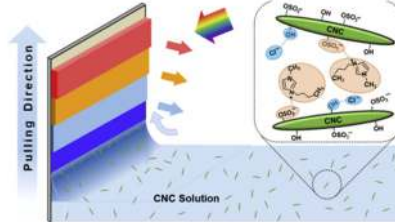
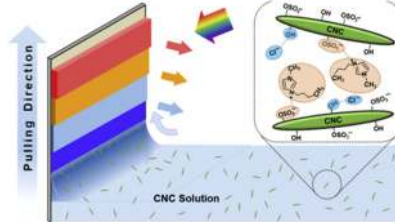
Detection Methods	Principle	Advantages	Disadvantages	Image	References
FET	Change in electrical behavior	Ultra-sensitive; adsorptive capacity; miniaturized; stability	Difficulties in fabrication; repeatability; high cost		A. Kukherjee et al. [47]
1.2. Electrochemical					
Amperometric	Measurement of electric current generated by chemical reactions in the electrochemical system.	Ultra-low power consumption; low cost; good selectivity; low detection limit; broad target gases; good for miniaturization	High maintenance if liquid electrolytes are used; interference may happen for some gases; slow response time		S. Achmann et al. [48]
1.3. Optical					
Evanescent	Change in absorption intensity	High sensitive, easy fabrication, low cost	Selectivity, repeatability		A. Prasanth et al. Reprinted with permission from Ref. [49] Copyright 2022 Elsevier
SPR	Shift in resonant frequency	High sensitive, selective	Cost of the materials used for fabrication, polarizers, cost of the spectrometers		V.R. Sudheer et al. [50]

Table 2. *Cont.*

Detection Methods	Principle	Advantages	Disadvantages	Image	References
LMR	Shift in resonant frequency	Easy fabrication, free from polarizers	Cost of the spectrometers		A. Prasanth et al. Reprinted with permission from Ref. [51] Copyright 2021 Elsevier
1.4. Acoustic					
SAW	Wave velocity and frequency travels on the surface drift as a change in the external environment	High sensitivity, fast response, room temperature operation, low cost	Restricted with low frequency, not suitable for liquid samples		J. Devkota et al. [52]
BAW	Wave velocity and frequency travels on the bulk drift as a change in the external environment	High sensitivity, robustness	Selectivity, costly		J. Hu et al. [53]
1.5. Colorimetric					A. Azzouz et al. Reprinted with permission from Ref. [54] Copyright 2019 Elsevier
GC-MS—gas chromatography–mass spectroscopy, PTR-MS—proton-transfer-reaction mass spectrometry, SIFT-MS—selected ion flow tube mass spectrometry, MID-IR—mid-infrared spectroscopy, PAS—photoacoustic, FET—field effect transistor, SPR—surface plasmon resonance, LMR—lossy mode resonance, SAW—surface acoustic wave, BAW—bulk acoustic wave.					

4. NM-Based Sensors—Potential Candidates for Disease Diagnosis

4.1. Diabetes Mellitus

In general, diabetes patients use fat instead of glucose for energy, and the liver produces ketones during fatty acid metabolism. However, the acceptable concentration of exhaled breath acetone in healthy individuals is less than 0.8 ppm, whereas it is higher than 1.8 ppm in diabetic patients. In this context, various nanoscale sensing materials have been explored for exhaled breath acetone sensing in the sub-ppm level.

For instance, Das et al. [55] grew thick films made of cobalt chromite (CoCr_2O_4) as shown in (Figure 2) to detect trace levels of acetone with high sensitivity along with rapid response/recovery time. The sensor showed poor cross-sensitivity towards other interferants including ammonia ethanol and humidity levels. The fabricated sensor showed an appreciable change for lower concentration levels of acetone vapors (1, 2, and 5 ppm) at 300°C . These thick film sensors show better stability and exhibit fast response and recovery times of 1.6 and 62 s, respectively. Other semiconductor metal oxides (SMO) such as SiO_2 , WO_3 , CuO , TiO_2 , and NiO have been exploited for acetone detection [56,57]. Recently, Hanh et al. [58] prepared ultrafine Pt nanoparticle-decorated Zn_2SO_4 (ZTO) hollow octahedra towards enhanced acetone sensing at the ppb level. Among all various Pt compositions, a 1 wt% Pt loading into ZTO exhibited an enhanced response towards acetone (~36.9-fold enhancement). Detecting acetone at the ppb level leads to exhaled breath-based diabetes detection. A Si-doped $\epsilon\text{-WO}_3$ nanostructured film-based portable sensor was developed and tested towards trace levels of acetone [59]. Brahma et al. [60] demonstrated a low concentration acetone sensor based on Cu-doped p-type ZnO nanostructures. The reported sensor showed prominent specificity towards acetone over other interferants at ambient temperatures. However, for the Cu-doped n-type ZnO nanostructures, the sensor response was poor. Kim et al. [61] grew a SnO_2 nanosheet with (101) crystal facets and tested it towards ppb level acetone sensing. The nanosheets were observed to have a high sheet area, which showed a nearly 10 times higher response than those synthesized for 2 h and 24 h. Thus, tailoring the crystal facet eventually enhances the sensor response characteristics without any noble metal addition. Furthermore, the potential of WO_3 nanocomposites to enhance the sensitivity and specificity towards acetone was reported by Imran et al. [62]. Xu et al. [63] synthesized WO_3 nanofibers and showed their excellent sensor response characteristics with a low detection limit. Yan et al. [64] studied the metabolic impacts of diabetes mellitus type 2 using GC-MS and found the potential biomarker has acetone with a threshold concentration of 1.8 ppm between healthy and diabetic patients. Koo et al. [65] and their research group synthesized $\text{Pd-ZnO/ZnCo}_2\text{O}_4$ hollow spheres followed by bimetallic MOFs and achieved a sensitivity of 69% towards acetone with a concentration of 5 ppm at 250°C . Zhang et al. [66] synthesized mulberry-shaped tin oxide (SnO_2) and samarium oxide (Sm_2O_3)-loaded tin oxide with different mol% (0.5, 1, 2.5, and 4) Sm_2O_3 . The 2.5 mol% $\text{Sm}_2\text{O}_3/\text{SnO}_2$ delivered a considerably enhanced sensor response (Ra/Rg , 41.14) to acetone with a low detection limit of 100 ppb. Wang et al. demonstrated high sensitivity and selectivity towards low acetone concentration in 90% RH using 10% Cr-doped $\epsilon\text{-WO}_3$ NPs [67]. Kim et al. [68] reported Rh_2O_3 NPs functionalized electrospun WO_3 nanofiber to detect acetone (1 ppm) in a relative humidity (RH) environment of 95%. Similarly, Shen et al. [69] synthesized carbon-doped WO_3 using a template method and observed excellent sensitivity, selectivity, and response time towards acetone in an RH environment. Moon et al. [70] fabricated a pristine hollow SnO_2 hemipill network (HSHN) and pt-functionalized (HPN) for detecting trace acetone levels. HPN showed a magnificent sensor response towards acetone over HSHN. HPN shows a lower LOD of 3.6 ppm towards 200 ppb of acetone under 80% RH. Nevertheless, Liu et al. [71] grew a $\text{ZnO-Bi}_2\text{O}_3$ nanosheets (NSs) heterostructure on the optical fiber using the sol-gel technique. The sensor exhibited good sensitivity, selectivity, and repeatability towards acetone with a detection limit of 140 ppb. Jiang et al. [72] developed a Yttrium Stabilized Zirconia (YSZ)-based mixed potential type acetone sensor along with Cd_2SnO_4 as the sensing electrode (SE). The proposed sensor was reliable for the pre-diagnosis of diabetes along

with good selectivity, repeatability, and long-term stability. Moreover, during clinical examination with the sample size of 25 exhaled breaths, the sensor showed an ability to distinguish between the healthy and diseased ones. The results indicated that the sensors were highly compatible for real-time clinical applications and showed 98% accuracy. Kim et al. [73] investigated the acetone-sensing properties of Ru-functionalized WO_3 NPs and showed a significant sensing response (78.61 for 5 ppm) and better selectivity towards acetone. Staerz et al. [74] fabricated a ketone sensor based on Rh_2O_3 - WO_3 heterojunctions and observed the surface doping enhances the acetone sensitivity. Guo et al. [75] used electrospinning combined with a hydrothermal technique to synthesize a cobalt oxide (Co_3O_4) nanofibers/cadmium sulfide (CdS) nanospheres sensor towards acetone detection. Figure 3 shows the schematic representation of the exhaled breath acetone sensor using a composite nanomaterial as the sensing material.

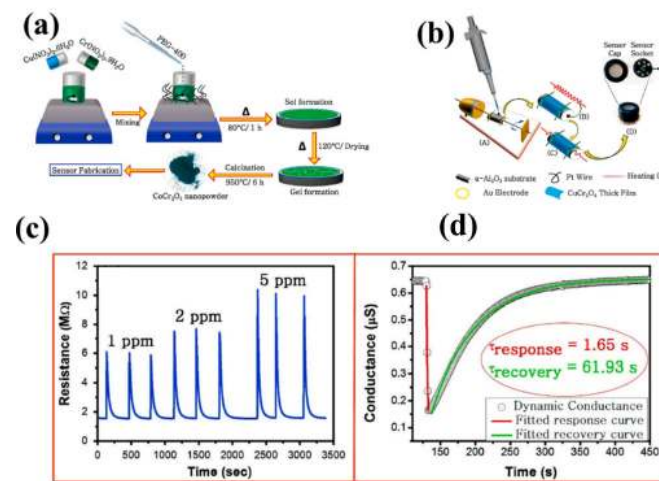


Figure 2. (a) Schematic illustration of the CoCr_2O_4 , (b) drop coating of the CoCr_2O_4 slurry on the sensor substrate, (c) dynamic response of the CoCr_2O_4 sensor to different traces of acetone vapor (d) transient conductance curve of the sensor by Langmuir absorption model at 300°C , Reprinted with permission from [55] Copyright 2021 Elsevier.

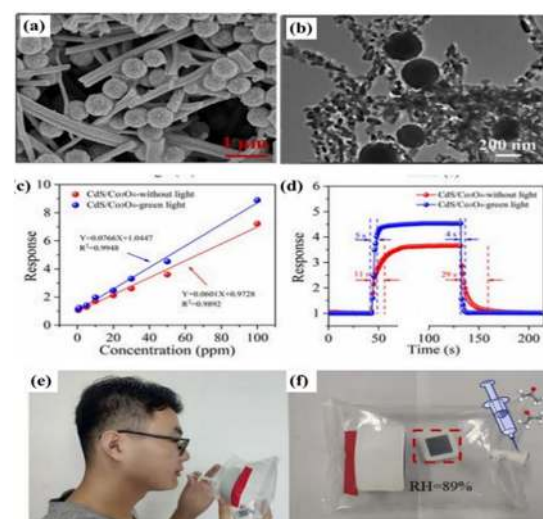


Figure 3. SEM and TEM images of (a,b) CdS/Co₃O₄ nanocomposite. (c) Curve fitting, (d) with and without the illumination of green light, response/recovery time of the CdS/Co₃O₄-based acetone sensor. The breath gas investigation of the Co₃O₄/CdS sensor. (e) Healthy experimenter breath sample is collected with air bag. (f) Injection of 2 ppm of acetone in to healthy people's exhaled breath Reprinted with permission from [75] Copyright 2022 Elsevier.

The CdS-Co₃O₄ composite sensor exhibits an excellent response towards acetone under green light irradiation (520 nm). The developed sensor is able to distinguish between healthy people and diabetic patients by detecting acetone in exhaled breath. Table 3 shows the comparison of various NM and its performance to lower concentrations of exhaled breath acetone at different operating conditions.

Table 3. Comparison of the selectivity, sensor response, and working temperature of the NM-based acetone gas sensor (effect of humidity is measured).

Materials	Concentration (ppm)	Response R _a /R _g	Selectivity (ppm)	T/°C	RH/%	Ref.
Co-doped ZnO nanofibers	5	5	4	360	25	Liu et al. [76]
Pd@ZnO	50	30	1.9	340	25	Xiao et al. [77]
Au/ZnO	5	15	1.7	270	NA	Wang et al. [78]
NiO-decorated ZnO	10	3.6	1.9	300	30	Liu et al. [79]
ZnO/ZnFe ₂ O ₄	5	9.4	2.4	250	NA	Ma et al. [80]
NiO/ZnO	1	1.3	2	275	30	Liu et al. [81]
ZnO nanosheets	5	6.7	2.5	300	40	Li et al. [82]
ZnO/ZnFe ₂ O ₄	1	3.2	1.9	290	NA	Wang et al. [83]
ZnO/ZnFe ₂ O ₄ microspheres	50	10	1.7	140	NA	Song et al. [84]
ZnO supercrystals	20	25.4	4.3	340	NA	Gong et al. [85]
La/ZnO nanoplates	50	25	1.8	330	24	Li et al. [86]
SnO ₂ nanowires	20	6	1.8	290	25	Qin et al. [87]
Pt@WO ₃	1	62	31	350	90	Kim et al. [88]

Chien et al. [89] developed an optical sensor, which could detect trace acetone concentrations based on the NADH fluorescence technique (Figure 4a,b). Exhaled breath samples from 25 diabetic and 55 healthy people were collected and showed the acetone levels of diabetic patients were higher (1207.7 ± 689.5 ppb) than those of healthy (750.0 ± 434.4 ppb) people (Figure 4c).

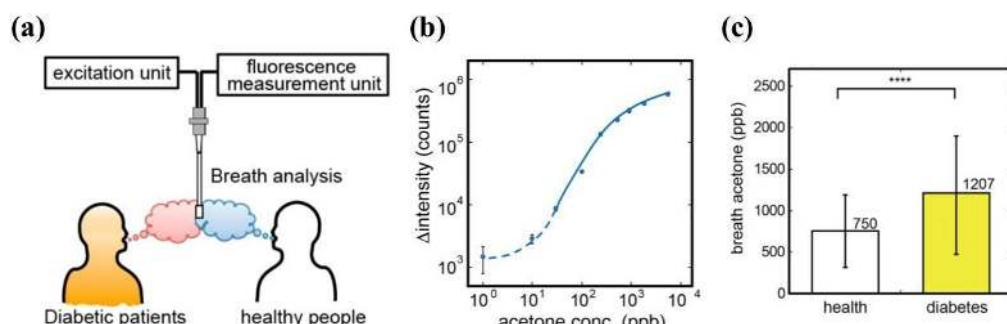


Figure 4. (a) Schematic representation. (b) Acetone biosniffers' sensitivity. (c) Healthy groups' and diabetic patients' exhaled breath acetone ($**** = p < 0.001$) Reprinted with permission from [89]. Copyright 2017 American Chemical Society.

4.2. Lung Cancer

A peroxidation of the cell membrane and the production of specific VOCs that are different from those produced by normal cells occur during tumor growth as a result of modifications to metabolic pathways, such as gene or protein changes. These VOCs can be found in the headspace of cancer cells or in the exhaled breath of cancer patients. VOCs are released by cancerous cells' blood, which then exchanges with air as it passes through the alveoli of the lungs [90]. The possibility of using VOCs found in patients' breath as diagnostic or screening tools has been thoroughly researched for a number of years. Chang et al. [91] developed a sensor device that uses seven SMO arrays (SnO₂) to detect lung cancer VOCs ethylbenzene, undecane, 4-methyloctane, 2,3,4-trimethylhexane, and 2,3,4-trimethylhexane with an RH of 80%, 5%, 16%, and 1%. The prepared sensor on this detecting system showed exclusive sensitivity to isobutane, toluene, and ethanol, as shown in Figure 5.

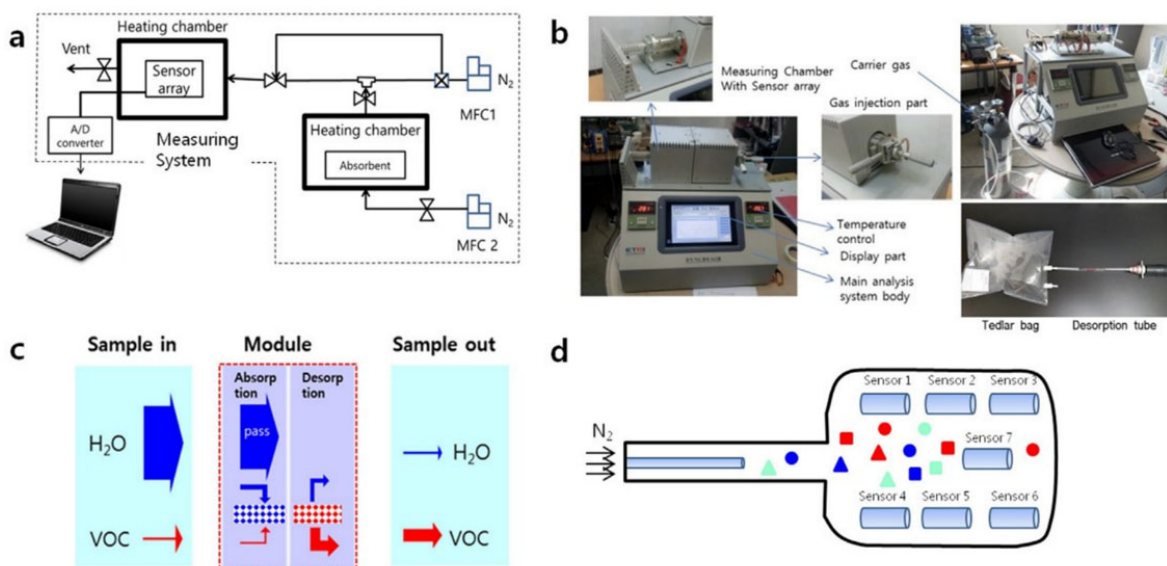


Figure 5. (a) Schematic of measurement system of exhaled breath analysis, (b) complete system photographs, (c) porous material based on 2,6-diphenylene oxide polymer is filled inside the desorption tubes, (d) and a delivery unit Reprinted with permission from [91] Copyright 2018 Elsevier.

Similarly, using polymer nanocomposites, S. Chatterjee et al. [92] demonstrated the operation of a room temperature electronic nose to detect lung cancer VOCs. Set 1 (acetone, water, methanol, ethanol, isopropanol, propanal, and 2-butanone) and Set 2 (chloroform, styrene, toluene, cyclohexane, benzene, n-propane, o-xylene, n-decane, isoprene, 1, 2, 4 trimethylbenzene, and 1-hexene). The sensor's sensitivity was adjusted by changing the composition of the polymer matrix with carbon nanotubes (CNT). The sensor system showed a shorter response time and lower LOD down to 2.5 ppm.

Z. Kahatoon et al. [93] analyzed the feasibility of doped SnO₂ nanomaterial towards acetone and toluene. Nanomaterial's such as undoped SnO₂, manganese (Mn), copper (Cu), chromium (Cr), and zinc (Zn)-doped SnO₂ were used as the sensing material. The high sensitivity of 0.19 μA/ppb was achieved in Cu-doped SnO₂ with a detection limit of 0.2 ppb. Peng et al. [94] constructed a sensor array comprising gold nanoparticles (GNPs) to perform ultra-low level gas detection. GNPs functionalized with organic functionalities were used as chemiresistor-based sensors for dodecanethiol, 2-ethyl hexanediol, decanethiol, tert-dodecanethiol, 1-butanethiol, hexanethiol, 4-methoxy-toluenethiol, 2-mercaptopbenzoxazole, and 11-mercapto-1-undecanol detection. Principal component analysis (PCA) observed the sensor array's sensing response. This sensing method detected no overlap between healthy VOCs and lung cancer VOCs. The same study group advanced the outstanding development of the sensor compared with other sensor arrays functionalized with carbon nanotubes. In addition, Hanh et al. [95] utilized the hollow cubic assembled nanocrystal Zn₂SO₄ to detect lung cancer VOCs. Targeted VOCs including acetone, ethanol, NH₃, methanol, carbon, and hydrogen monoxide were passed over the sensing layer at 350 °C and 450 °C, and the result showed the maximum sensor response to ethanol and acetone gases, as shown in Figure 6. The sensor response was 47.80% for 125 ppm of acetone and 7.52% for 10 ppm of ethanol underneath 450 °C. The LOD was found to be 175 ppb. Furthermore, the prepared sensor reveals that acetone is more sensitive at 450 °C than 350 °C.

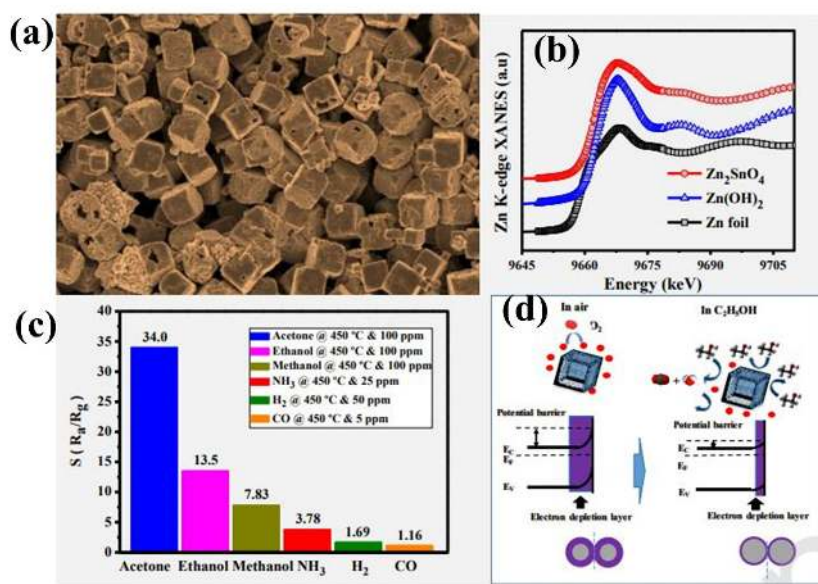


Figure 6. Zn_2SnO_4 hollow cubic assembled for lung cancer VOC biomarker **(a)** Zn_2SnO_4 SEM image, **(b)** first derivative XANES Spectra of Zn_2SnO_4 , **(c)** Selectivity, **(d)** Gas sensing mechanism. Reprinted with permission from [95] Copyright 2020 Elsevier.

Q. Chen et al. [96] developed the flexible electronic e-nose, assembling graphene oxide with different ratios of metal ions (M^{X+}). This group conducted a case study of real-time exhaled breath analysis using different nanomaterial-coated sensors. The system contained different sensing nanomaterials (rGO-ctrl, rGO-Co, rGO-Ce, rGO-Fe, rGO-Cu) that clearly distinguished the healthy control with 95.8% sensitivity and 96.0% specificity, as indicated in Figure 7. Table 4 represents the various NM used to detect exhaled breath lung cancer biomarkers.

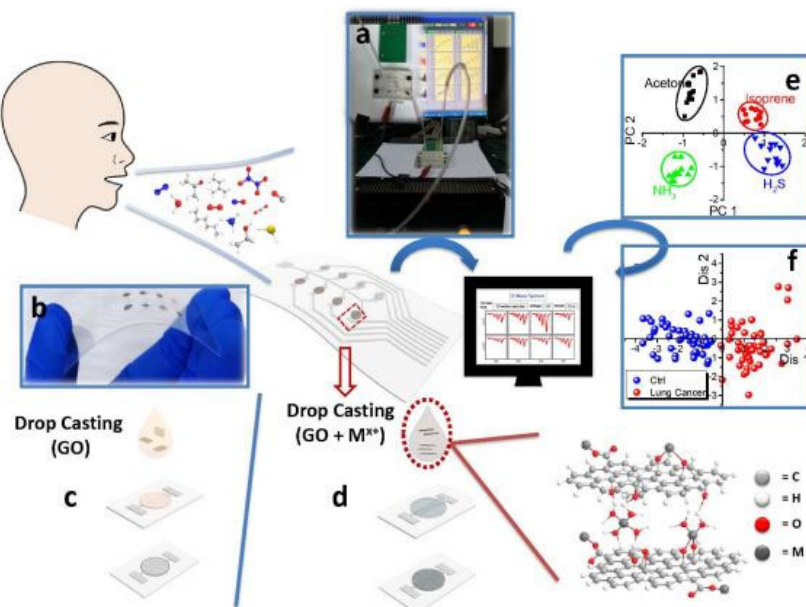


Figure 7. An overview of e-nose system comprising the metal ion induced assembly of rGO; **(a)** E-nose system photograph, **(b)** rGO-m, **(c)** Drop casting comparison of GO, **(d)** M^{X+} induced assembled GO, **(e)** Pattern recognition by PCA, **(f)** clinical EB analysis by linear discrimination analysis. Reprinted with permission from [96] Copyright 2020 American Chemical Society.

Table 4. Various biomarkers and methodology/NM used towards lung cancer exhaled breath analysis.

No.	Method/NM	VOC Biomarkers	Reference
1	Calorimetric/AuNR-MTPP	decane; hexanal; undecane; benzene; heptanal; and 1,2,4-trimethylbenzene	Huo et al. [97]
2	Chemiresistive/WO ₃ Nanofiber and composites	Hydrogen sulfide and toluene	Kim et al. [98]
3	Chemiresistive/ZnO and graphene	Acetone	Liu et al. [99]
4	Chemiresistive/functionalized β-cyclodextrin wrapped with rGO	Acetone; benzene; methanol; ethanol; formaldehyde; toluene; xylene; propional; isopropanol	Nag et al. [100]
5	Chemiresistive/sulfonated poly nanocomposites based on hybrid nanocarbons	Methanol; ethanol; propanol; acetone; butanone; benzene; toluene; water	Nag et al. [101]
6	Chemiresistive/sensor array	Styrene; α-phellandrene; dodecane; 4-methyl	Agmon et al. [102]
7	Chemiresistive/WO ₃ -0.33H ₂ O, hexagonal-WO ₃ , and their reduced graphene oxide composites	Acetone; benzene; methanol; toluene; m-xylene	Perfecto et al. [103]
8	UV light irradiation/WO ₃ nanowire doped with Pt, Au, Ni, Fe	Exhaled breath	Saidi et al. [104]
9	Chemiresistive method/carbon nanorods, PLA/CNR, PVA/CNR	Acetone; diethyl ether; carbon disulfide; acetonitrile; benzaldehyde; benzyl alcohol; trimethyl benzene; ethyl benzene; benzene; toluene; xylene; cyclohexane; hexene-1; 2-methyl-1-propanol; isopropanol; methanol; ethanol; water; formaldehyde	Tripathi et al. [105]
10	Chemiresistor/NP thin film	Acetone and hexane + acetone mixture	Zhao et al. [106]
11	Chemiresistive/porphyrin and its derivatives	p-xylene; styrene; isoprene and hexanal	Zhao et al. [107]
12	Optical LMR/poly[methyl(3,3,3-trifluoropropyl) siloxane] (PMTFPS)	ethane; benzene; heptane; toluene; octane; pentane; styrene and decane.	Silva et al. [108]
13	Optical LMR/Silver NP	Inhale and exhale Analysis	Rivero et al. [109]
14	Optical LMR/organometallic [Au ₂ Ag ₂ (C ₆ F ₅) ₄ (NH ₃) ₂] _n	Methanol; ethanol and isopropanol	Elosua et al. [110]
15	Optical LMR/[Au ₂ Ag ₂ (C ₆ F ₅) ₄ (C ₆ H ₅ C CC ₆ H ₅) ₂] _n	Methanol; ethanol and isopropanol	Elosua et al. [111]

rGO—reduced graphene oxide, CNR—carbon nanorods, PVA—poly(vinyl acetate), NP—nanoparticle, LMR—lossy mode resonance, PLA—poly(lactic acid), MTPP—metalloporphyrins.

Daneshkhah et al. [112] utilized the poly(vinylidene fluoride-hexafluoropropylene) (PVDF-HFP) to detect VOCs including water, acetone, ethanol, isoprene, and 2-ethylhexyl acetate. Sensor 1 (PVDF-HFP/C65) confirmed 52.6% resistance to acetone, while the isoprene, ethanol, and 2-EHA responses were 5.6%, 3%, and 0.11%, respectively. Sensor 2 (two layers of PVDF-HFP, PVDF-HFP/C65) was arranged using a spin-coating technique, which resulted in a good response time. Comparatively, sensor 2 showed a much lower reaction time than sensor 1, 52% for acetone, 92% for water, and 61% for isoprene. In sensor 3, CNT was brought into conjunction with PVDF-HFP/C65/CNT to increase resistance while uncovered to air. That was in contrast to sensors 1 and 2, in which the performance of sensor 3 showed growth in resistance and a quick response time. In addition, Gragis et al. [113] used auxiliary devices mounted on a silicon substrate, and a commercial semiconductor gas sensor based on SnO₂ was used in the prototype. Toluene, o-xylene, propanol, and cyclohexane were the four biomarkers. The total performance evaluation was carried out with various primary elements, i.e., the studies were carried out in dry environments and without CO₂, at temperatures below 25 °C. Second, the effect of water vapor and CO₂ was investigated. The sensor device accurately calculated the reaction time in under a minute. The technique has successfully detected toluene, o-xylene, and propanol with detection limits of 24, 5, and 21 ppb, respectively. In addition to chemiresistive-based sensors, FOS has been used to detect VOC concentrations due to their quick reaction and ease of manufacture.

4.3. Breast Cancer

The breast cancer biomarkers are linked to oxidative stress in the breast cancer tissues, resulting from an imbalance between free radicals and the antioxidant species. The oxidative stress increases the reactive oxygen species production resulting in the peroxidation of polyunsaturated fatty acids in the cell membranes, releasing the alkanes and their derivatives released in the exhaled breath [114]. Zhang et al. [115] reported an ultrathin quasi-2D PANI (polyaniline)-based conducting polymer for diagnosing breast cancer VOCs heptanal (10 ppm) and others as low as 30 ppb.

The chemiresistive sensing mechanism of the q2D PANI sensor shows that an increase in heptanal concentration increases the electrical resistance of the sensing material. Peng et al. [116] studied the breath analysis using the GC-MS technique and compared the obtained volatile signatures of breast cancer patients using the GNP sensor array. The following observations were made on breath analysis using the GNP sensor array: no pretreatment was required, faster results, discriminated the healthy and the cancer patient volatile signatures, and other breath components. The reported GNP sensor array can be an alternative diagnostic tool for diagnosing breast and other cancer biomarkers. The GNP sensor array is portable, cost-effective, and non-invasive. Katwal et al. [117] fabricated ZnO nanotube–nanowire-based hybrid structures and studied their response towards breast cancer VOCs such as 2-propanol, heptanal, isopropyl myristate, and acetophenone. The chemiresistive sensing response of the hybrid structure exhibited a nominal response to breast cancer-related VOCs. The fabricated sensor responded better to acetophenone at 250 °C compared to the other VOCs. Konvalina et al. [118] discussed the effective use of NM-based volatile sensors for discriminating healthy and diseased individuals. They detected trace level exhaled breath VOCs and discussed optimizing an NM-based sensor platform to reduce the redundancy produced by the real-world environmental condition and other noisy breath components. Upon solving the drawbacks, the proposed chemiresistive sensors can be integrated into the chips on a smartphone for remote monitoring. Barash et al. [119] discriminated against the genetic mutations of breast cancer with breast volatomics. They compared the exhaled breath sample patterns using GC-MS to an array of cross-reactive GNPs and SWCNT along with different organic layers, as shown in Figure 8. The results indicate that discriminant function analysis (DFA)-based responses from the GNP sensor array have a better accuracy of 83% in discriminating breast cancer and non-breast cancer patients than GC-MS analysis. Table 5 represents the comparison of various exhaled breath breast cancer biomarkers and their respective detection techniques used.

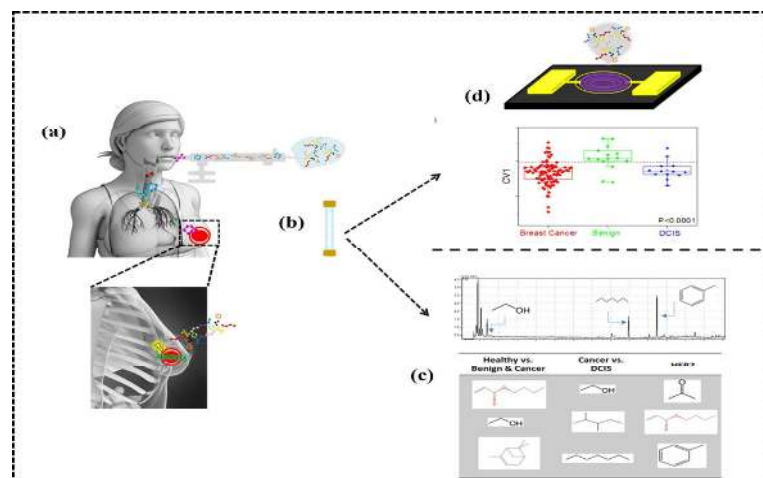


Figure 8. (a) Exhalation and sample collection, (b) concentrated on Tenax® TA sorption tubes, (c) GC-MS analysis of the collected sample, (d) exposed to nanosensor array [119].

Table 5. Various biomarkers and their relevant functional group specific towards breast cancer.

No.	Detection Technique	Functional Group	VOC Biomarkers	Ref.
1	GC-MS	Alkane	Pentane; H ₂ O ₂ ; pentanol; hexanol 3-methylhexane; decane; caryophyllene;	Phillips et al. [114]
2	GC-MS	Alkane	naphthalene; and trichloroethylene	Mangler et al. [120]
3	GC-MS	n-Alkane	Ethane; pentane 2-amino-5-isopropyl-8-methyl-1-	Phillips et al. [121]
4	GC-MS	n-Methyl Alkane	azulenecarbonitrile; 3,3-dimethyl pentane; 5-(2-methylpropyl)nonane; 6-ethyl-3-octyl ester 2-trifluoromethyl benzoic acid; 2,3,4-trimethyl decane;	Schmidt et al. [122]
5	Nanowire-based chemiresistive sensor array	Aldehyde; alkane	2,3-dihydro-1-phenyl-4(1H)-quinazolinone; isopropyl myristate; 2-propanol; 1-phenyl-ethanone; heptanal; Cyclohexane; dodecane; pentadecane;	Sun et al. [123]
6	GC-MS	Alkane; aldehyde	heptanal; 2-propanol; etc.,	Silva et al. [124]
7	GC-MS	Alkene	1-hexadecanol; 5-(z)-dodecenioic acid	Tanaka et al. [125]
8	GC-MS	Alkane	2,5,6-trimethyl octane; 1,4-dimethoxy-2,3 butanediol; cyclohexane 2-hexyl-1-octanol; tridecane; benzene;	Cai et al. [126]
9	GC-MS	Alcohol; alkane; aromatic	1,2,4,5-tetramethyl; 2,5-Cyclohexadiene-1,4-dione; 2,6-bis(1,1-dimethylethyl); cyclopropane; ethylidene	Phillips et al. [127]
10	GC-MS	Alkane	heptanal; dodecane; nonadecane; 3-methyl; octane; pentadecane; 6-methyl; propane; 2-methyl; tridecane; 5-methyl; 4-methyl; nonane; 2-methyl;	Phillips et al. [128]
11	GC-MS	Alkane; ketone; alcohol;	2,3-dihydro-1-phenyl-4(1H)-quinazolinone; and isopropyl myristate; 2-propanol; 1-phenyl-ethanone;	Phillips et al. [129]

4.4. Kidney Diseases

Hemodialysis is a treatment process for end-stage renal disease, which is expensive and time-consuming. However, the exhaled breath-based diagnosis technique can be a potential tool for early-stage disease diagnosis, reducing the number of hemodialysis cases. The exhaled breath NH₃ concentration can be a significant parameter in determining the different stages of renal cancer. Additionally, the exhaled NH₃ can be used for the diagnoses of Helicobacter pylori and liver disease.

Guntner et al. [130] reported that Si-doped α -MoO₃ has better selectivity towards NH₃ at sub-ppm levels with different RH% levels. The breath NH₃ concentration of the healthy individual is 0.96 ppm, and for the end-stage renal disease (ESRD) patients, it ranges from 4.9 ppm upwards. Li et al. [131] observed that by tuning, the sensing temperature of MoO₃ can be selective towards NH₃ compared to other gas H₂S. This is due to the acid-base interaction between acidic MoO₃ and primary NH₃/amines. Yu et al. [132] used a P₃HT-based polymer gas sensor to study the breath NH₃ concentration before and after hemodialysis and the blood urea nitrogen tests. Based on the above observation, the correlation between blood urea nitrogen and breath NH₃ was 0.96. Maout et al. [133] used a polyaniline-based nanocomposite sensor array to determine NH₃ concentration (500–2100 ppb) in exhaled breath. In that array, sensor 1 (polyaniline/chitosan) nanocomposite, sensor 4 (polyaniline/TiO₂) nanocomposite, and sensor 5 (polyaniline/CNT) nanocomposite, shown in Figure 9, had better response characteristics towards lower concentrations of NH₃. Then the sensor results were fed to different classification algorithms to determine the sensor performance towards NH₃ compared to other interfering factors. Some of the nanomaterial-coated ammonia sensors are listed in Table 6.

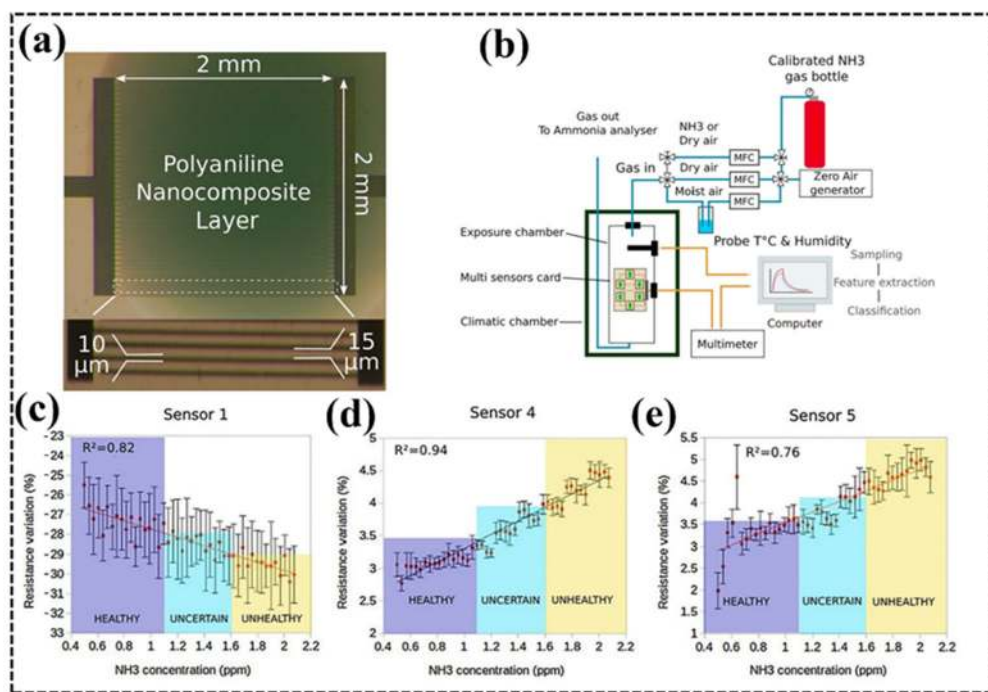


Figure 9. (a) NH₃ sensor. (b) Senor test bench schematic. (c) Resistance vs NH₃ concentration for (d) sensor 1—polyaniline/chitosan nanocomposite, (e) sensor 4—polyaniline/TiO₂ nanocomposite, (f) sensor 5—polyaniline/CNT nanocomposite Reprinted with permission from [133] Copyright 2018 Elsevier.

Table 6. Various nanomaterials towards NH₃ biomarkers and their research group.

No.	Nanomaterial	VOC Biomarkers	Ref.
1	Si-doped α-MoO ₃	NH ₃ , H ₂ S	Li et al. [131]
2	P ₃ HT-based polymer	NH ₃	Yu et al. [132]
3	Polyaniline nanocomposite	NH ₃	Maout et al. [133]
4	RGO-SnO ₂	NH ₃	R.Ghosh et al. [134]
5	SnO ₂	NH ₃	A.Pathak et al. [135]
6	Gadolinium-doped tin oxide	NH ₃	S. Maheswari et al. [136]
7	ITO-SWCNT	NH ₃	F. Rigoni et al. [137]

4.5. Halitosis

Though halitosis has various origins, 90% of patients have volatile sulfide (methanethiol and hydrogen sulfide) in their oral cavity. These sulfides can be generated by *Helicobacter pylori*, and are related to halitosis. Hydrogen sulfide (H₂S) is a potential biomarker for halitosis in exhaled breath. Thus selective detection of H₂S in exhaled breath is required to differentiate healthy and halitosis patients. Accordingly, Feng et al. [138] grew NiO/WO₃ nanoparticles (NPs) for selective and sensitive detection of H₂S. Markedly, 2.1 wt% NiO/WO₃ NPs showed high sensitivity to H₂S, which was nearly 43 times greater than pristine WO₃ NPs at the same operating conditions, as shown in Figure 10. Furthermore, the developed composite sensor showed a lower LOD of 0.05 ppm with greater selectivity. Hu et al. [139] fabricated an H₂S sensor based on a flower-like MoO₃/WO₃ composite. The gas sensors based on Mo₆W exhibited a better sensor response of 28.5%, a quick response/recovery time (2 s/5 s), a LOD of 20 ppb, and excellent selectivity at a temperature of 250 °C. Shin et al. [140] attempted facile co-functionalization of WO₃ nanofibers with alkaline metal (Na) and noble metal (Pt) catalysts via an electrospinning process. The developed sensor was used for direct and measurable study of halitosis. The relationship between the H₂S gas and breath signs acquired by the sensing device (80 cases) and gas chromatography showed excellent accuracy of 86.3%.

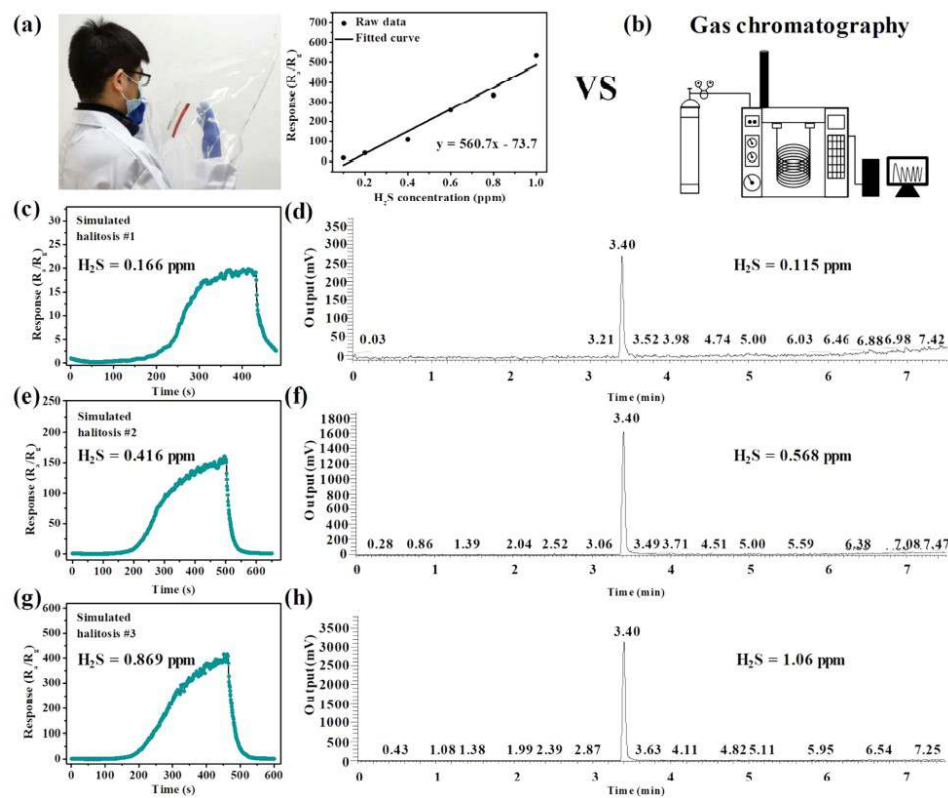


Figure 10. (a) Photo of NiO/WO₃ NP sensor prototype's collection of exhaled breath and its response. (b) For the comparison, the gas chromatography setup is used. The corresponding sensor response of prototype to (c) simulated halitosis no. 1, (e) simulated halitosis no. 2, and (g) simulated halitosis no. 3. The gas chromatogram corresponding results for (d) simulated halitosis no. 1, (f) simulated halitosis no. 2, and (h) simulated halitosis no. 3 Reprinted/adapted with permission from Ref. [138]. Copyright 2021 American Chemical Society.

4.6. COVID-19

According to the WHO coronavirus disease report 189, severe acute respiratory syndrome coronavirus-2 (SARS-CoV-2, aka COVID-19) caused 650,000 deaths in more than 197 countries worldwide within seven months. Due to late detection and severe infection, approximately 97.5% of patient's headway COVID-19 symptoms occurred in 11.5 days. A gold standard molecular test for SARS-CoV-2 is used to confirm the presence of COVID-19. A swab sample and a time-consuming laboratory process are required in order to follow conventional techniques. Because of the shipping of samples and the overcrowding of laboratories, test results can be delayed for many days, adding to the healthcare system's burden. According to epidemiological data based on viral RNA sequences, the COVID-19 spread can be attributed to personal identifiable information. Only by developing rapid, low-cost, and simple-to-use diagnostics for identifying the infection at an earlier stage, even before symptoms appear, will the significant increase in infection be reduced. In dealing with the COVID-19 epidemic, various sensor and biosensor approaches have recently been addressed, emphasizing the need for a point of care device. Some possible solutions have already been proposed, for example, B. Shan et al. [141] presented a sensor array based on nanomaterial with multiplexing capabilities for a COVID-19 detection and exhaled breath monitoring system. To analyze the breath, samples the nanomaterial sensor array is used, which comprises cross-reactive chemiresistive sensors based on spherical gold nanoparticles of diameter 3–4 nm with different organic ligands as the reactive layer. G. Qui et al. [142] developed a plasmonic-based biosensor that combines the plasmonic photothermal (PPT) effect and the sensing mechanism of localized surface plasmon resonance (LSPR). The detection of SARS-CoV-2 used a functional material such as a two-dimensional

gold nanoisland (AuNIs) functionalized with complementary DNA receptors. Ethyl butyrate (EB) was recognized in recent research as a prominent biomarker of COVID-19, as EB content was higher in COVID-19 patients' exhaled breath. The electronic activities of the EB molecules of pristine, Al-, and Si-doped BC3 nanosheets were investigated using density functional theory [143]. K. Snitz et al. [144] developed a point of care real-time sensing device consisting of a stainless-steel chamber (volume: 1.8 mL, temperature: 110 °C) with 10 different thermoregulated metal oxide sensors. An interaction of compounds on the sensor results in an oxygen exchange that changes electrical conductivity. Receiver operating characteristic curves (ROCs) of 0.58 and 0.63 were obtained. D.K. Nuruputra et al. [145] developed a portable electronic e-nose system utilizing an array of metal oxide semiconductors (GeNose C19) to detect COVID-19 from exhaled breath, as shown in Figure 11.

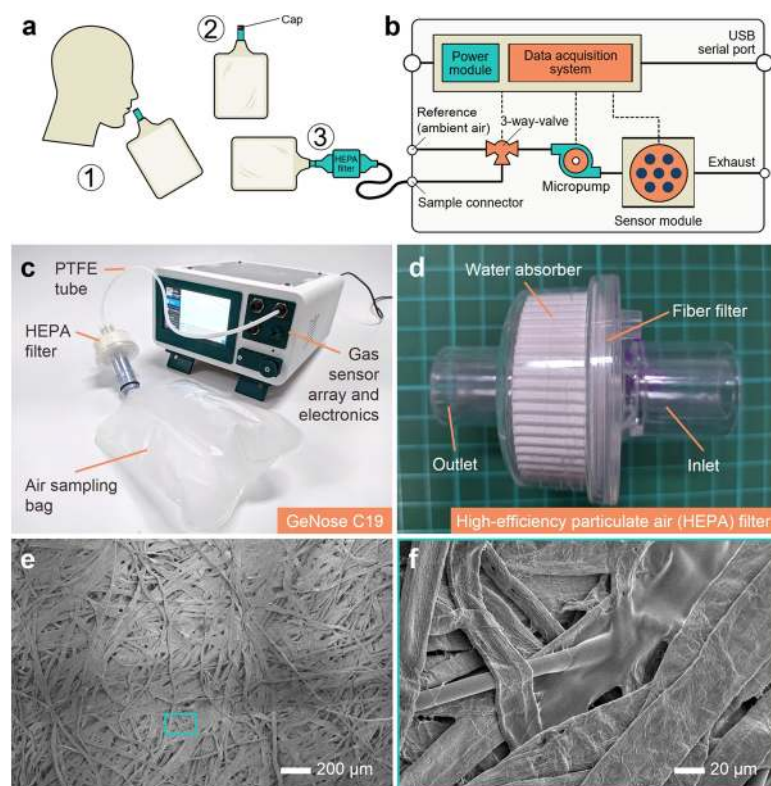


Figure 11. (a) Schematic of the GeNose C19 off-line breath sampling pipeline: (1) inhaling air via the nose and then exhaling it through the mouth into a sampling bag, (2) sealing or shutting the sampling bag lid to prevent collected air leakage, and (3) directly inserting the sampling bag into the electronic nose inlet. (b,c) GeNose C19 integrated with a high-efficiency particulate air (HEPA) filter and an air sample bag through a flexible medical-grade polytetrafluoroethylene (PTFE) tube with a 4 mm outer diameter. The electronic nose is made up of numerous major electrical and mechanical components. The sensor module is made up of ten separate sensing devices stacked in an array. (d) HEPA filter for removing particulates and trapping SARS-CoV-2 from the exhaled breath of a patient verified to have positive COVID-19. (e,f) SEM images of the fiber filter [145].

5. Summary and Conclusions

In conclusion, the potential of various NM-based sensor technologies for disease diagnosis was reviewed, and various studies on breath analysis discussed. Sensing materials with extremely high selectivity for precise biomarker gases or an array of sensing materials that exhibit different sensing behaviors to sets of multiple biomarker gases are required to diagnose diseases from exhaled breath. As sensing materials, a variety of nanomaterials with distinct sensing properties, such as SMO, CNT, graphene-based materials, and poly-

mers, can be used. Specifically, catalyst-loaded SMO and their arrays have typically been used for diabetic detection via the acetone level in breath. Similarly, due to the combined effects of an increased active surface area and significant electrocatalytic activity, metal ion composites with SMO-based chemiresistive sensors favor the selective detection of lung cancer VOCs, whereas a gold NP-based chemiresistive sensor array can be a potential alternative for spectroscopic-based techniques for the detection of cancer VOCs from the breath. WO_3 , Mo, and their composites towards sulfur are highly sensitive and selective, and are capable of reproducible sensing of H_2S and the diagnosis of halitosis. Catalyst-doped MoO_3 has a high tendency to detect NH_3 to diagnose renal disease. However, the conventional ways of quantifying VOC through spectroscopic techniques may result in certain disadvantages such as a difficulty in attaining singular VOC patterns. However, these nanomaterial-based techniques are cost-effective, have ease of fabrication, and are portable. In addition, these nanomaterials can be tuned with different materials for the selective detection of various gases. Researchers have successfully demonstrated disease diagnosis containing numerous biomarkers using nanomaterial-based sensor arrays.

Nevertheless, a new hybrid and blended approach with tuning of the optimal parameters should be developed to achieve better sensitivity, selectivity, and precision. For successive exhaled breath analysis, humidity and temperature interference of various sensing characteristics must be reduced to negligible levels. Pretreatment components such as dehumidifiers, preconcentrators during breath sample collection, and flow sensors must be technologically advanced in order to use breath analysis in real-time applications. As a result, clinical professionals diagnosing patients, chemists or materials scientists designing sensing materials, and MEMS experts designing embedded primary treatment components should collaborate to design pretreatment and sensing components concurrently.

6. Future Prospects

Looking into future prospects, since breath analysis for disease diagnosis is an interdisciplinary field, it necessitates the collaboration of scientists from material science, information technology, sensor technology, and medical diagnostics. A tremendous effort will be required to commercialize such breath sensor devices along with miniaturization, calibration, and batch production in the market so that wellbeing can be observed quickly and easily, and patients can be screened at an initial disease stage.

Considering wearability and skin attachability, strain-insensitive flexible sensors with supreme data transmission are of paramount importance in any future system. Data fusion from different sensor sources is also an efficient way to obtain reliable information from each sensor with less uncertainty. To cope with sensor data handling, classification, and acquisition, various advanced algorithm models such as PCA, KNN, ANN, and LDA have been exploited with trade-offs between computation speed and accuracy. In addition, artificial intelligence and IoT compatible sensors have made patient-friendly smart-cloud medical systems, which could be a viable option for real-time diagnosis, initial care, and the allocation of a suitable source of medical care.

Author Contributions: Conceptualization, M.V., A.P. and Z.C.A.; formal analysis, M.V., A.P., S.N., S.R.M. and Z.C.A.; writing—original draft, M.V., A.P. and S.N.; resource, M.V., A.P. and S.N.; data curation, M.V., A.P. and S.N.; writing—review and editing, A.C., A.S., S.R.M., S.R., E.R. and Z.C.A.; methodology, S.R.M. and Z.C.A.; visualization, S.R.M. and Z.C.A.; supervision, Z.C.A. All authors have read and agreed to the published version of the manuscript.

Funding: This work was supported under the project MHRD SPARC [SPARC/2018-2019/P461/SL].

Institutional Review Board Statement: Not applicable.

Informed Consent Statement: Not applicable.

Data Availability Statement: The authors confirm that the data supporting the findings of this study are available within the article.

Acknowledgments: The authors acknowledge DST- FIST and MHRD SPARC, India, for providing financial support through the projects [SR/FST/ETI-015/2011] and [SPARC/2018-2019/P461/SL] for carrying out the present investigation.

Conflicts of Interest: The authors declare no conflict of interest.

References

1. Pleil, J.D.; A Stiegel, M.; Sobus, J.R.; Liu, Q.; Madden, M.C. Observing the human exposome as reflected in breath biomarkers: Heat map data interpretation for environmental and intelligence research. *J. Breath Res.* **2011**, *5*, 037104. [[CrossRef](#)] [[PubMed](#)]
2. Bouza, M.; Gonzalez-Soto, J.; Pereiro, R.; De Vicente, J.C.; Sanz-Medel, A. Exhaled Breath and Oral Cavity VOCs as Potential Biomarkers in Oral Cancer Patients. *J. Breath Res.* **2017**, *11*, 016015. [[CrossRef](#)] [[PubMed](#)]
3. Phillips, M. Breath Tests in Medicine. *Sci. Am.* **1992**, *267*, 74–79. [[CrossRef](#)]
4. Campanella, A.; De Summa, S.; Tommasi, S. Exhaled breath condensate biomarkers for lung cancer. *J. Breath Res.* **2019**, *13*, 044002. [[CrossRef](#)]
5. Kim, K.-H.; Jahan, S.A.; Kabir, E. A review of breath analysis for diagnosis of human health. *TrAC Trends Anal. Chem.* **2012**, *33*, 1–8. [[CrossRef](#)]
6. Biagini, D.; Lomonaco, T.; Ghimenti, S.; Bellagambi, F.G.; Onor, M.; Scali, M.C.; Barletta, V.; Marzilli, M.; Salvo, P.; Trivella, M.G.; et al. Determination of volatile organic compounds in exhaled breath of heart failure patients by needle trap micro-extraction coupled with gas chromatography-tandem mass spectrometry. *J. Breath Res.* **2017**, *11*, 047110. [[CrossRef](#)]
7. Miekisch, W.; Herbig, J.; Schubert, J. Data interpretation in breath biomarker research: Pitfalls and directions. *J. Breath Res.* **2012**, *6*, 036007. [[CrossRef](#)]
8. Pleil, J.D.; Wallace, M.A.G.; Stiegel, M.A.; Funk, W.E. Human biomarker interpretation: The importance of intra-class correlation coefficients (ICC) and their calculations based on mixed models, ANOVA, and variance estimates. *J. Toxicol. Environ. Heal. Part B* **2018**, *21*, 161–180. [[CrossRef](#)]
9. Konvalina, G.; Haick, H. Sensors for Breath Testing: From Nanomaterials to Comprehensive Disease Detection. *Accounts Chem. Res.* **2013**, *47*, 66–76. [[CrossRef](#)]
10. Cheng, W.-H.; Lee, W.-J. Technology development in breath microanalysis for clinical diagnosis. *J. Lab. Clin. Med.* **1999**, *133*, 218–228. [[CrossRef](#)]
11. Beauchamp, J. Inhaled today, not gone tomorrow: Pharmacokinetics and environmental exposure of volatiles in exhaled breath. *J. Breath Res.* **2011**, *5*, 037103. [[CrossRef](#)] [[PubMed](#)]
12. Kim, I.-D. How can nanotechnology be applied to sensors for breath analysis? *Nanomedicine* **2017**, *12*, 2695–2697. [[CrossRef](#)] [[PubMed](#)]
13. Zhang, C.-L.; Yu, S.-H. Nanoparticles meet electrospinning: Recent advances and future prospects. *Chem. Soc. Rev.* **2014**, *43*, 4423–4448. [[CrossRef](#)] [[PubMed](#)]
14. Braun, P.X.; Gmachl, C.F.; Dweik, R.A. Bridging the Collaborative Gap: Realizing the Clinical Potential of Breath Analysis for Disease Diagnosis and Monitoring—Tutorial. *IEEE Sensors J.* **2012**, *12*, 3258–3270. [[CrossRef](#)]
15. Espinal, L.; Poster, D.L.; Wong-Ng, W.; Allen, A.J.; Green, M.L. Measurement, standards, and data needs for CO₂capture materials: A critical review. *Environ. Sci. Technol.* **2013**, *47*, 11960–11975. [[CrossRef](#)]
16. Huang, J.; Li, Y.; Sood, S.; Gouma, P. Breath Biomarker Detection by Chemical Sensors. In *Semiconductor-Based Sensors*; World Scientific: Singapore, 2016; pp. 355–393. [[CrossRef](#)]
17. Vishinkin, R.; Haick, H. Nanoscale Sensor Technologies for Disease Detection via Volatolomics. *Small* **2015**, *11*, 6142–6164. [[CrossRef](#)]
18. Novak, B.J.; Blake, D.R.; Meinardi, S.; Rowland, F.S.; Pontello, A.; Cooper, D.M.; Galassetti, P.R. Exhaled methyl nitrate as a noninvasive marker of hyperglycemia in type 1 diabetes. *Proc. Natl. Acad. Sci. USA* **2007**, *104*, 15613–15618. [[CrossRef](#)]
19. Galassetti, P.R.; Novak, B.; Nemet, D.; Rose-Gottron, C.; Cooper, D.M.; Meinardi, S.; Newcomb, R.; Zaldivar, F.; Blake, D.R. Breath Ethanol and Acetone as Indicators of Serum Glucose Levels: An Initial Report. *Diabetes Technol. Ther.* **2005**, *7*, 115–123. [[CrossRef](#)]
20. Hakim, M.; Broza, Y.Y.; Barash, O.; Peled, N.; Phillips, M.; Amann, A.; Haick, H. Volatile Organic Compounds of Lung Cancer and Possible Biochemical Pathways. *Chem. Rev.* **2012**, *112*, 5949–5966. [[CrossRef](#)]
21. Zhang, Y.; Guo, L.; Qiu, Z.; Lv, Y.; Chen, G.; Li, E. Early Diagnosis of Breast Cancer from Exhaled Breath by Gas Chromatography-Mass Spectrometry (GC/MS) Analysis: A Prospective Cohort Study. *J. Clin. Lab. Anal.* **2020**, *34*, 1–10. [[CrossRef](#)]
22. Phillips, M.; Cataneo, R.N.; Saunders, C.; Hope, P.; Schmitt, P.; Wai, J. Volatile biomarkers in the breath of women with breast cancer. *J. Breath Res.* **2010**, *4*, 026003. [[CrossRef](#)] [[PubMed](#)]
23. Choi, K.-I.; Kim, H.-J.; Kang, Y.C.; Lee, J.-H. Ultrasensitive detection of H₂S in highly humid atmosphere using cuo-loaded SNO₂ hollow spheres for real-time diagnosis of halitosis. *Sens. Actuators B Chem.* **2014**, *194*, 371–376. [[CrossRef](#)]
24. Španěl, P.; Smith, D. What is the real utility of breath ammonia concentration measurements in medicine and physiology? *J. Breath Res.* **2017**, *12*, 027102. [[CrossRef](#)] [[PubMed](#)]
25. Obermeier, J.; Trefz, P.; Happ, J.; Schubert, J.K.; Staude, H.; Fischer, D.-C. Exhaled volatile substances mirror clinical conditions in pediatric chronic kidney disease. *PLoS ONE* **2017**, *12*, e0178745. [[CrossRef](#)] [[PubMed](#)]

26. Lü, Q.; Zhang, Q.; Kang, S.; Bai, H.; Wang, C. [Determination of 10 volatile organic compounds in toys by headspace gas chromatography-mass spectrometry]. *Chin. J. Chromatogr.* **2010**, *28*, 800–804. [[CrossRef](#)]
27. Feng, D.; Wang, J.; Ji, X.-J.; Min, W.-X.; Yan, W.-J. Analysis of Volatile Organic Compounds by HS-GC-IMS in Powdered Yak Milk Processed under Different Sterilization Conditions. *J. Food Qual.* **2021**, *2021*, 5536645. [[CrossRef](#)]
28. Vu, D.C.; Ho, T.L.; Vo, P.H.; Carlo, G.; McElroy, J.A.; Davis, A.N.; Nagel, S.C.; Lin, C.-H. Determination of volatile organic compounds in child care centers by thermal desorption gas chromatography-mass spectrometry. *Anal. Methods* **2018**, *10*, 730–742. [[CrossRef](#)]
29. Vu, D.C.; Ho, T.L.; Vo, P.; Bayati, M.; Davis, A.N.; Gulseven, Z.; Carlo, G.; Palermo, F.; McElroy, J.A.; Nagel, S.C.; et al. Assessment of indoor volatile organic compounds in Head Start child care facilities. *Atmospheric Environ.* **2019**, *215*, 116900. [[CrossRef](#)]
30. Curran, K.; Underhill, M.; Gibson, L.T.; Strlic, M. The development of a SPME-GC/MS method for the analysis of VOC emissions from historic plastic and rubber materials. *Microchem. J.* **2016**, *124*, 909–918. [[CrossRef](#)]
31. Bai, J.; Liu, S.; Xie, F.; Liu, H.; Xia, Q. [Analysis of volatile and semi-volatile compounds in tobacco using off-line combination of liquid chromatography and capillary gas chromatography-mass spectrometry]. *Chin. J. Chromatogr.* **2010**, *28*, 608–614. [[CrossRef](#)]
32. Woollam, M.; Teli, M.; Angarita-Rivera, P.; Liu, S.; Siegel, A.; Yokota, H.; Agarwal, M. Detection of Volatile Organic Compounds (VOCs) in Urine via Gas Chromatography-Mass Spectrometry QTOF to Differentiate Between Localized and Metastatic Models of Breast Cancer. *Sci. Rep.* **2019**, *9*, 2526. [[CrossRef](#)] [[PubMed](#)]
33. Lourenço, C.; Bergin, S.; Hodgkinson, J.; Francis, D.; Staines, S.E.; Saffell, J.R. Instrumentation for quantitative analysis of volatile compounds emission at elevated temperatures. part 1: Design and implementation. *Sci. Rep.* **2020**, *10*, 8700. [[CrossRef](#)] [[PubMed](#)]
34. Westhoff, M.; Litterst, P.; Freitag, L.; Urfer, W.; Bader, S.; Baumbach, J.-I. Ion mobility spectrometry for the detection of volatile organic compounds in exhaled breath of patients with lung cancer: Results of a pilot study. *Thorax* **2009**, *64*, 744–748. [[CrossRef](#)]
35. Bessa, V.; Darwiche, K.; Teschler, H.; Sommerwerck, U.; Rabis, T.; Baumbach, J.I.; Freitag, L. Detection of volatile organic compounds (VOCs) in exhaled breath of patients with chronic obstructive pulmonary disease (COPD) by ion mobility spectrometry. *Int. J. Ion Mobil. Spectrom.* **2011**, *14*, 7–13. [[CrossRef](#)]
36. Güntner, A.T.; Abegg, S.; Königstein, K.; Gerber, P.A.; Schmidt-Trucksäss, A.; Pratsinis, S.E. Breath Sensors for Health Monitoring. *ACS Sens.* **2019**, *4*, 268–280. [[CrossRef](#)]
37. Mirzaei, A.; Leonardi, S.G.; Neri, G. Detection of hazardous volatile organic compounds (voCs) by metal oxide nanostruc-tures-based gas sensors: A Review. *Ceram. Int.* **2016**, *42*, 15119–15141. [[CrossRef](#)]
38. Khatoon, Z.; Fouad, H.; Seo, H.-K.; Alothman, O.Y.; Ansari, Z.A.; Ansari, S.G. Ethyl acetate chemical sensor as lung cancer bi-omarker detection based on doped nano-sno₂ synthesized by sol-gel process. *IEEE Sens. J.* **2020**, *20*, 12504–12511. [[CrossRef](#)]
39. Wang, J.; Han, S.; Ke, D.; Wang, R. Semiconductor Quantum Dots Surface Modification for Potential Cancer Diagnostic and Therapeutic Applications. *J. Nanomater.* **2012**, *2012*, 129041. [[CrossRef](#)]
40. Velumani, M.; Meher, S.R.; Alex, Z.C. Impedometric humidity sensing characteristics of SnO₂ thin films and SnO₂–ZnO composite thin films grown by magnetron sputtering. *J. Mater. Sci. Mater. Electron.* **2017**, *29*, 3999–4010. [[CrossRef](#)]
41. Gao, F.; Wang, M.; Zhang, X.; Zhang, J.; Xue, Y.; Wan, H.; Wang, P. Simultaneous detection of hydrogen and methane in breath for the diagnosis of small intestinal bacterial overgrowth by fast gas chromatography. *Anal. Methods* **2018**, *10*, 4329–4338. [[CrossRef](#)]
42. Jung, Y.J.; Seo, H.S.; Kim, J.H.; Song, K.Y.; Park, C.H.; Lee, H.H. Advanced Diagnostic Technology of Volatile Organic Compounds Real Time analysis Analysis From Exhaled Breath of Gastric Cancer Patients Using Proton-Transfer-Reaction Time-of-Flight Mass Spectrometry. *Front. Oncol.* **2021**, *11*, 560591. [[CrossRef](#)] [[PubMed](#)]
43. Ruzsanyi, V.; Mochalski, P.; Schmid, A.; Wiesenhofer, H.; Klieber, M.; Hinterhuber, H. Ion mobility spectrometry for de-tection of Skin Volatiles. *J. Chromatogr. B* **2012**, *911*, 84–92. [[CrossRef](#)] [[PubMed](#)]
44. Rodrigues, J.; Amin, A.; Raghushaker, C.R.; Chandra, S.; Joshi, M.B.; Prasad, K.; Nayak, S.G.; Ray, S.; Mahato, K.K. Exploring photoacoustic spectroscopy-based machine learning together with metabolomics to assess breast tumor progression in a xen-ograft model ex vivo. *Lab. Investigig.* **2021**, *101*, 952–965. [[CrossRef](#)] [[PubMed](#)]
45. Tan, X.; Zhang, H.; Li, J.; Wan, H.; Guo, Q.; Zhu, H.; Liu, H.; Yi, F. Non-dispersive infrared multi-gas sensing via nanoantenna integrated narrowband detectors. *Nat. Commun.* **2020**, *11*, 5245. [[CrossRef](#)] [[PubMed](#)]
46. Acharyya, S.; Nag, S.; Kimbahune, S.; Ghose, A.; Pal, A.; Guha, P.K. Selective Discrimination of VOCs Applying Gas Sensing Kinetic Analysis over a Metal Oxide-Based Chemiresistive Gas Sensor. *ACS Sensors* **2021**, *6*, 2218–2224. [[CrossRef](#)] [[PubMed](#)]
47. Mukherjee, A.; Rosenwaks, Y. Recent Advances in Silicon FET Devices for Gas and Volatile Organic Compound Sensing. *Chemosensors* **2021**, *9*, 260. [[CrossRef](#)]
48. Achmann, S.; Hämmeler, M.; Moos, R. Amperometric enzyme-based gas sensor for formaldehyde: Impact of possible interferences. *Sensors* **2008**, *8*, 1351–1365. [[CrossRef](#)]
49. Prasanth, A.; Meher, S.; Alex, Z. Metal oxide thin films coated evanescent wave based fiber optic VOC sensor. *Sensors Actuators A: Phys.* **2022**, *338*, 113459. [[CrossRef](#)]
50. Kaushik, S.; Tiwari, U.K.; Deep, A.; Sinha, R. Two-dimensional transition metal dichalcogenides assisted biofunctionalized optical fiber SPR biosensor for efficient and rapid detection of bovine serum albumin. *Sci. Rep.* **2019**, *9*, 6987. [[CrossRef](#)]
51. Prasanth, A.; Meher, S.; Alex, Z. Experimental analysis of SnO₂ coated LMR based fiber optic sensor for ethanol detection. *Opt. Fiber Technol.* **2021**, *65*, 102618. [[CrossRef](#)]
52. Devkota, J.; Ohodnicki, P.R.; Greve, D.W. SAW Sensors for Chemical Vapors and Gases. *Sensors* **2017**, *17*, 801. [[CrossRef](#)] [[PubMed](#)]

53. Hu, J.; Qu, H.; Pang, W.; Duan, X. In-line detection with microfluidic bulk acoustic wave resonator gas sensor for Gas Chromatography. *Sensors* **2021**, *21*, 6800. [[CrossRef](#)] [[PubMed](#)]
54. Azzouz, A.; Vikrant, K.; Kim, K.-H.; Ballesteros, E.; Rhadfi, T.; Malik, A.K. Advances in colorimetric and optical sensing for gaseous volatile organic compounds. *TrAC Trends Anal. Chem.* **2019**, *118*, 502–516. [[CrossRef](#)]
55. Das, S.; Mahapatra, P.L.; Mondal, P.P.; Das, T.; Pal, M.; Saha, D. A highly sensitive cobalt chromite thick film based trace acetone sensor with fast response and recovery times for the detection of diabetes from exhaled breath. *Mater. Chem. Phys.* **2021**, *262*, 124291. [[CrossRef](#)]
56. Daneshnazar, M.; Jaleh, B.; Eslamipanah, M.; Varma, R.S. Optical and Gas Sensing Properties of TiO₂/RGO for Methanol, Ethanol and Acetone Vapors. *Inorg. Chem. Commun.* **2022**, *145*, 110014. [[CrossRef](#)]
57. Singh, I.; Bedi, R.K. Ethanol, acetone and ammonia gas room temperature operated sensor. *AIP Conf. Proc.* **2013**, *1536*, 1175. [[CrossRef](#)]
58. Hanh, N.H.; Van Duy, L.; Hung, C.M.; Xuan, C.T.; Van Duy, N.; Hoa, N.D. High-performance acetone gas sensor based on Pt-Zn₂SnO₄ hollow octahedra for diabetic diagnosis. *J. Alloys Compd.* **2021**, *886*, 161284. [[CrossRef](#)]
59. Righetto, M.; Tricoli, A.; Gass, S.; Schmid, A.; Amann, A.; Pratsinis, S.E. Breath acetone monitoring by portable Si:WO₃ gas sensors. *Anal. Chim. Acta* **2012**, *738*, 69–75. [[CrossRef](#)]
60. Brahma, S.; Yeh, Y.; Huang, J.; Liu, C. CU-doped zinc oxide fiber optic sensor for acetone detection at room temperature. *Appl. Phys. A* **2020**, *126*, 718.
61. Kim, K.; Choi, P.G.; Itoh, T.; Masuda, Y. Catalyst-free Highly Sensitive SnO₂ Nanosheet Gas Sensors for Parts per Billion-Level Detection of Acetone. *ACS Appl. Mater. Interfaces* **2020**, *12*, 51637–51644. [[CrossRef](#)]
62. Imran, M.; Rashid, S.S.A.A.H.; Sabri, Y.; Motta, N.; Tesfamichael, T.; Sonar, P.; Shafiei, M. Template based sintering of WO₃ nanoparticles into porous tungsten oxide nanofibers for acetone sensing applications. *J. Mater. Chem. C* **2019**, *7*, 2961–2970. [[CrossRef](#)]
63. Xu, H.; Gao, J.; Li, M.; Zhao, Y.; Zhang, M.; Zhao, T.; Wang, L.; Jiang, W.; Zhu, G.; Qian, X.; et al. Mesoporous WO₃ Nanofibers With Crystalline Framework for High-Performance Acetone Sensing. *Front. Chem.* **2019**, *7*, 266. [[CrossRef](#)] [[PubMed](#)]
64. Yan, Y.; Wang, Q.; Li, W.; Zhao, Z.; Yuan, X.; Huang, Y.; Duan, Y. Discovery of potential biomarkers in exhaled breath for diagnosis of type 2 diabetes mellitus based on GC-MS with metabolomics. *RSC Adv.* **2014**, *4*, 25430–25439. [[CrossRef](#)]
65. Koo, W.-T.; Choi, S.-J.; Jang, J.-S.; Kim, I.-D. Metal-Organic Framework Templated Synthesis of Ultrasmall Catalyst Loaded ZnO/ZnCo₂O₄ Hollow Spheres for Enhanced Gas Sensing Properties. *Sci. Rep.* **2017**, *7*, srep45074. [[CrossRef](#)]
66. Zhang, Y.; Zhou, L.; Liu, Y.; Liu, D.; Liu, F.; Liu, F.; Yan, X.; Liang, X.; Gao, Y.; Lu, G. Gas sensor based on samarium oxide loaded mulberry-shaped tin oxide for highly selective and sub ppm-level acetone detection. *J. Colloid Interface Sci.* **2018**, *531*, 74–82. [[CrossRef](#)]
67. Wang, L.; Teleki, A.; Pratsinis, S.E.; Gouma, P.I. Ferroelectric WO₃ Nanoparticles for Acetone Selective Detection. *Chem. Mater.* **2008**, *20*, 4794–4796. [[CrossRef](#)]
68. Kim, N.-H.; Choi, S.-J.; Kim, S.-J.; Cho, H.-J.; Jang, J.-S.; Koo, W.-T. Highly sensitive and selective acetone sensing performance of WO₃ nanofibers functionalized by rh2o3 nanoparticles. *Sens. Actuators B Chem.* **2016**, *224*, 185–192. [[CrossRef](#)]
69. Shen, J.-Y.; Zhang, L.; Ren, J.; Wang, J.-C.; Yao, H.-C.; Li, Z.-J. Highly enhanced acetone sensing performance of porous C-doped WO₃ hollow spheres by carbon spheres as templates. *Sens. Actuators B Chem.* **2017**, *239*, 597–607. [[CrossRef](#)]
70. Moon, H.G.; Jung, Y.; Jun, D.; Park, J.H.; Chang, Y.W.; Park, H.-H. Hollow Pt-functionalized SnO₂ hemipill network formation using a bacterial skeleton for the noninvasive diagnosis of diabetes. *ACS Sens.* **2018**, *3*, 661–669. [[CrossRef](#)]
71. Liu, W.; Zheng, Y.; Wang, Z.; Wang, Z.; Yang, J.; Chen, M. Ultrasensitive exhaled breath sensors based on anti-resonant hollow core fiber with in situ grown zno-bi2O₃ nanosheets. *Adv. Mater. Interfaces* **2021**, *8*, 2001978. [[CrossRef](#)]
72. Jiang, L.; Lv, S.; Tang, W.; Zhao, L.; Wang, C.; Wang, J.; Wang, T.; Guo, X.; Liu, F.; Wang, C.; et al. YSZ-based acetone sensor using a Cd2SnO₄ sensing electrode for exhaled breath detection in medical diagnosis. *Sens. Actuators B Chem.* **2021**, *345*, 130321. [[CrossRef](#)]
73. Kim, K.-H.; Kim, S.-J.; Cho, H.-J.; Kim, N.-H.; Jang, J.-S.; Choi, S.-J.; Kim, I.-D. WO₃ nanofibers functionalized by protein-templated RuO₂ nanoparticles as highly sensitive exhaled breath gas sensing layers. *Sens. Actuators B Chem.* **2017**, *241*, 1276–1282. [[CrossRef](#)]
74. Staerz, A.; Kim, T.H.; Lee, J.H.; Weimar, U.; Barsan, N. Nanolevel Control of Gas Sensing Characteristics via P-n Heterojunction between Rh₂O₃ Clusters and WO₃ Crystallites. *J. Phys. Chem. C* **2017**, *121*, 24701–24706. [[CrossRef](#)]
75. Guo, J.; Zhang, D.; Li, T.; Zhang, J.; Yu, L. Green light-driven acetone gas sensor based on electrospun CdS nanospheres/Co₃O₄ nanofibers hybrid for the detection of exhaled diabetes biomarker. *J. Colloid Interface Sci.* **2021**, *606*, 261–271. [[CrossRef](#)] [[PubMed](#)]
76. Liu, L.; Li, S.; Zhuang, J.; Wang, L.; Zhang, J.; Li, H.; Liu, Z.; Han, Y.; Jiang, X.; Zhang, P. Improved selective acetone sensing properties of Co-doped ZnO nanofibers by electrospinning. *Sens. Actuators B Chem.* **2011**, *155*, 782–788. [[CrossRef](#)]
77. Xiao, Y.; Lu, L.; Zhang, A.; Zhang, Y.; Sun, L.; Huo, L. Highly enhanced acetone sensing performances of porous and single crystalline zno nanosheets: High percentage of exposed (100) facets working together with surface modification with pd na-noparticles. *ACS Appl. Mater. Interfaces* **2012**, *4*, 3797–3804. [[CrossRef](#)]
78. Wang, X.-J.; Wang, W.; Liu, Y.-L. Enhanced acetone sensing performance of Au nanoparticles functionalized flower-like ZnO. *Sens. Actuators B Chem.* **2012**, *168*, 39–45. [[CrossRef](#)]
79. Liu, C.; Wang, B.; Liu, T.; Sun, P.; Gao, Y.; Liu, F. Facile synthesis and gas sensing properties of the flower-like NIO-decorated zno microstructures. *Sens. Actuators B Chem.* **2016**, *235*, 294–301. [[CrossRef](#)]

80. Ma, X.; Zhou, X.; Gong, Y.; Han, N.; Liu, H.; Chen, Y. MOF-derived hierarchical $\text{ZnO}/\text{ZnFe}_2\text{O}_4$ hollow cubes for enhanced acetone gas-sensing performance. *RSC Adv.* **2017**, *7*, 34609–34617. [\[CrossRef\]](#)
81. Liu, C.; Zhao, L.; Wang, B.; Sun, P.; Wang, Q.; Gao, Y.; Liang, X.; Zhang, T.; Lu, G. Acetone gas sensor based on NiO/ZnO hollow spheres: Fast response and recovery, and low (ppb) detection limit. *J. Colloid Interface Sci.* **2017**, *495*, 207–215. [\[CrossRef\]](#)
82. Li, S.-M.; Zhang, L.-X.; Zhu, M.-Y.; Ji, G.-J.; Zhao, L.-X.; Yin, J.; Bie, L.-J. Acetone sensing of ZnO nanosheets synthesized using room-temperature precipitation. *Sens. Actuators B Chem.* **2017**, *249*, 611–623. [\[CrossRef\]](#)
83. Wang, X.; Zhang, S.; Shao, M.; Huang, J.; Deng, X.; Hou, P.; Xu, X. Fabrication of $\text{ZnO}/\text{ZnFe}_2\text{O}_4$ hollow nanocages through metal organic frameworks route with enhanced gas sensing properties. *Sens. Actuators B Chem.* **2017**, *251*, 27–33. [\[CrossRef\]](#)
84. Song, X.-Z.; Qiao, L.; Sun, K.-M.; Tan, Z.; Ma, W.; Kang, X.-L. Triple-shelled $\text{ZnO}/\text{ZnFe}_2\text{O}_4$ heterojunctional hollow micro-spheres derived from Prussian blue analogue as high-performance acetone sensors. *Sens. Actuators B Chem.* **2018**, *256*, 374–382. [\[CrossRef\]](#)
85. Gong, F.; Peng, L.; Zhang, Y.; Cao, Y.; Jia, D.; Li, F. Selectively sensing H_2S and acetone through tailoring the facets exposed on the surfaces of ZnO supercrystals. *Mater. Lett.* **2018**, *218*, 106–109. [\[CrossRef\]](#)
86. Li, Y.; Chen, L.-L.; Lian, X.-X.; Li, J. Formation Mechanism and Gas-Sensing Performance of La/ZnO Nanoplates Synthesized by a Facile Hydrothermal Method. *J. Electron. Mater.* **2018**, *47*, 2970–2978. [\[CrossRef\]](#)
87. Qin, L.; Xu, J.; Dong, X.; Pan, Q.; Cheng, Z.; Xiang, Q.; Li, F. The template-free synthesis of square-shaped SnO_2 nanowires: The temperature effect and acetone gas sensors. *Nanotechnology* **2008**, *19*, 185705. [\[CrossRef\]](#)
88. Kim, S.; Choi, S.; Jang, J.; Kim, N.; Hakim, M.; Tuller, H.L.; Kim, D. Mesoporous WO_3 nanofibers with protein-templated nanoscale catalysts for detection of trace biomarkers in exhaled breath. *ACS Nano* **2016**, *10*, 5891–5899. [\[CrossRef\]](#)
89. Chien, P.-J.; Suzuki, T.; Tsujii, M.; Ye, M.; Minami, I.; Toda, K.; Otsuka, H.; Toma, K.; Arakawa, T.; Araki, K.; et al. Biochemical Gas Sensors (Biosniffers) Using Forward and Reverse Reactions of Secondary Alcohol Dehydrogenase for Breath Isopropanol and Acetone as Potential Volatile Biomarkers of Diabetes Mellitus. *Anal. Chem.* **2017**, *89*, 12261–12268. [\[CrossRef\]](#)
90. Ratiu, A.; Ligor, T.; Bintintan, V.B.; Mayhew, C.A.; Buszewski, B. Volatile organic compounds in exhaled breath as fingerprints of lung cancer, Asthma and COPD. *J. Clin. Med.* **2021**, *10*, 32. [\[CrossRef\]](#)
91. Chang, J.-E.; Lee, D.-S.; Ban, S.-W.; Oh, J.; Jung, M.Y.; Kim, S.-H.; Park, S.; Persaud, K.; Jheon, S. Analysis of volatile organic compounds in exhaled breath for lung cancer diagnosis using a sensor system. *Sens. Actuators B Chem.* **2018**, *255*, 800–807. [\[CrossRef\]](#)
92. Chatterjee, S.; Castro, M.; Feller, J.F. An e-nose made of carbon nanotube based quantum resistive sensors for the detection of eighteen polar/nonpolar VOC biomarkers of lung cancer. *J. Mater. Chem. B* **2013**, *1*, 4563–4575. [\[CrossRef\]](#) [\[PubMed\]](#)
93. Khatoon, Z.; Fouad, H.; Seo, H.K.; Hashem, M.; Ansari, Z.A.; Ansari, S.G. Feasibility study of doped SnO_2 nanomaterial for electronic nose towards sensing biomarkers of lung cancer. *J. Mater. Sci. Mater. Electron.* **2020**, *31*, 15751–15763. [\[CrossRef\]](#)
94. Peng, G.; Tisch, U.; Adams, O.; Hakim, M.; Shehada, N.; Broza, Y.Y.; Billan, S.; Abdah-Bortnyak, R.; Kuten, A.; Haick, H. Diagnosing lung cancer in exhaled breath using gold nanoparticles. *Nat. Nanotechnol.* **2009**, *4*, 669–673. [\[CrossRef\]](#) [\[PubMed\]](#)
95. Hanh, N.H.; Van Duy, L.; Hung, C.M.; Van Duy, N.; Heo, Y.-W.; Van Hieu, N.; Hoa, N.D. VOC gas sensor based on hollow cubic assembled nanocrystal Zn_2SnO_4 for breath analysis. *Sensors Actuators A: Phys.* **2020**, *302*, 111834. [\[CrossRef\]](#)
96. Chen, Q.; Chen, Z.; Liu, D.; He, Z.; Wu, J. Constructing an E-nose using metal-ion-induced assembly of graphene oxide for diagnosis of lung cancer via exhaled breath. *ACS Appl. Mater. Interfaces* **2020**, *12*, 17713–17724. [\[CrossRef\]](#)
97. Huo, D.; Xu, Y.; Hou, C.; Yang, M.; Fa, H. A Novel Optical Chemical sensor based AUNR-MTPP and dyes for lung cancer biomarkers in exhaled breath identification. *Sens. Actuators B Chem.* **2014**, *199*, 446–456. [\[CrossRef\]](#)
98. Kim, N.-H.; Choi, S.-J.; Yang, D.-J.; Bae, J.; Park, J.; Kim, I.-D. Highly sensitive and selective hydrogen sulfide and toluene sensors using Pd functionalized WO_3 nanofibers for potential diagnosis of halitosis and lung cancer. *Sens. Actuators B Chem.* **2014**, *193*, 574–581. [\[CrossRef\]](#)
99. Liu, L.; Zhang, D.; Zhang, Q.; Chen, X.; Xu, G.; Lu, Y.; Liu, Q. Smartphone-based sensing system using ZnO and graphene modified electrodes for VOCs detection. *Biosens. Bioelectron.* **2017**, *93*, 94–101. [\[CrossRef\]](#)
100. Nag, S.; Sachan, A.; Castro, M.; Choudhary, V.; Feller, J. Spray layer-by-layer assembly of POSS functionalized CNT quantum chemo-resistive sensors with tuneable selectivity and ppm resolution to VOC biomarkers. *Sens. Actuators B Chem.* **2015**, *222*, 362–373. [\[CrossRef\]](#)
101. Nag, S.; Castro, M.; Choudhary, V.; Feller, J.-F. Sulfonated poly(ether ether ketone) [SPEEK] nanocomposites based on hybrid nanocarbons for the detection and discrimination of some lung cancer VOC biomarkers. *J. Mater. Chem. B* **2016**, *5*, 348–359. [\[CrossRef\]](#)
102. Montuschi, P. Exhaled breath condensate: A new approach to monitoring lung inflammation. In *New Perspectives in Monitoring Lung Inflammation*; CRC Press: Boca Raton, FL, USA, 2004; pp. 15–24.
103. Perfecto, T.M.; Zito, C.A.; Volanti, D.P. Room-temperature volatile organic compounds sensing based on $\text{WO}_3 \cdot 0.33\text{H}_2\text{O}$, hexagonal- WO_3 , and their reduced graphene oxide composites. *RSC Adv.* **2016**, *6*, 105171–105179. [\[CrossRef\]](#)
104. Saidi, T.; Palmowski, D.; Babicz-Kiewlicz, S.; Welearegay, T.G.; El Bari, N.; Ionescu, R.; Smulko, J.; Bouchikhi, B. Exhaled breath gas sensing using pristine and functionalized WO_3 nanowire sensors enhanced by UV-light irradiation. *Sens. Actuators B Chem.* **2018**, *273*, 1719–1729. [\[CrossRef\]](#)
105. Tripathi, K.; Sachan, A.; Castro, M.; Choudhary, V.; Sonkar, S.; Feller, J. Green carbon nanostructured quantum resistive sensors to detect volatile biomarkers. *Sustain. Mater. Technol.* **2018**, *16*, 1–11. [\[CrossRef\]](#)

106. Zhao, W.; Al-Nasser, L.F.; Shan, S.; Li, J.; Skeete, Z.; Kang, N.; Luo, J.; Lu, S.; Zhong, C.-J.; Grausgruber, C.J.; et al. Detection of mixed volatile organic compounds and lung cancer breaths using chemiresistor arrays with crosslinked nanoparticle thin films. *Sens. Actuators B Chem.* **2016**, *232*, 292–299. [[CrossRef](#)]
107. Zhao, S.; Lei, J.; Huo, D.; Hou, C.; Luo, X.; Wu, H.; Fa, H.; Yang, M. A colorimetric detector for lung cancer related volatile organic compounds based on cross-response mechanism. *Sens. Actuators B Chem.* **2018**, *256*, 543–552. [[CrossRef](#)]
108. Silva, L.I.B.; Freitas, A.C.; Rocha-Santos, T.A.P.; Pereira, M.E.; Duarte, A.C. Breath analysis by optical fiber sensor for the de-termination of exhaled organic compounds with a view to diagnostics. *Talanta* **2011**, *83*, 1586–1594. [[CrossRef](#)]
109. Rivero, P.J.; Urrutia, A.; Goicoechea, J.; Arregui, F. Optical fiber humidity sensors based on Localized Surface Plasmon Resonance (LSPR) and Lossy-mode resonance (LMR) in overlays loaded with silver nanoparticles. *Sens. Actuators B Chem.* **2012**, *173*, 244–249. [[CrossRef](#)]
110. Elosua, C.; Arregui, F.; Zamarreño, C.; Bariain, C.; Luquin, A.; Laguna, M.; Matias, I.R. Volatile organic compounds optical fiber sensor based on lossy mode resonances. *Sens. Actuators B Chem.* **2012**, *173*, 523–529. [[CrossRef](#)]
111. Elosúa, C.; Vidondo, I.; Arregui, F.J.; Bariain, C.; Luquin, A.; Laguna, M. Lossy mode resonance optical fiber sensor to detect organic vapors. *Sens. Actuators B Chem.* **2013**, *187*, 65–71. [[CrossRef](#)]
112. Daneshkhah, A.; Shrestha, S.; Agarwal, M.; Varahramyan, K. Poly(vinylidene fluoride-hexafluoropropylene) composite sensors for volatile organic compounds detection in breath. *Sens. Actuators B Chem.* **2015**, *221*, 635–643. [[CrossRef](#)]
113. Gregis, G.; Sanchez, J.-B.; Bezverkhyy, I.; Guy, W.; Berger, F.; Fierro, V. Detection and quantification of lung cancer bi-omarkers by a micro-analytical device using a single metal oxide-based Gas Sensor. *Sens. Actuators B Chem.* **2018**, *255*, 391–400. [[CrossRef](#)]
114. Phillips, M.; Bevers, T.B.; Larsen, L.H.; Pappas, N.; Pathak, S. Rapid point-of-care breath test predicts breast cancer and abnormal mammograms in symptomatic women. *medRxiv* **2020**. [[CrossRef](#)]
115. Zhang, T.; Qi, H.; Liao, Z.; Horev, Y.D.; Panes-Ruiz, L.A.; Petkov, P.S.; Zhang, Z.; Shivhare, R.; Zhang, P.; Liu, K.; et al. Engineering crystalline quasi-two-dimensional polyaniline thin film with enhanced electrical and chemiresistive sensing performances. *Nat. Commun.* **2019**, *10*, 4225. [[CrossRef](#)]
116. Peng, G.; Hakim, M.; Broza, Y.Y.; Billan, S.; Abdah-Bortnyak, R.; Kuten, A.; Tisch, U.; Haick, H. Detection of lung, breast, colorectal, and prostate cancers from exhaled breath using a single array of nanosensors. *Br. J. Cancer* **2010**, *103*, 542–551. [[CrossRef](#)]
117. Katwal, G.; Paulose, M.; Rusakova, I.A.; Martinez, J.E.; Varghese, O.K. Rapid Growth of Zinc Oxide Nanotube–Nanowire Hybrid Architectures and Their Use in Breast Cancer-Related Volatile Organics Detection. *Nano Lett.* **2016**, *16*, 3014–3021. [[CrossRef](#)] [[PubMed](#)]
118. Konvalina, G.; Haick, H. Effect of Humidity on Nanoparticle-Based Chemiresistors: A Comparison between Synthetic and Real-World Samples. *ACS Appl. Mater. Interfaces* **2012**, *4*, 317–325. [[CrossRef](#)] [[PubMed](#)]
119. Barash, O.; Zhang, W.; Halpern, J.M.; Hua, Q.-L.; Pan, Y.-Y.; Kayal, H.; Khouri, K.; Liu, H.; Davies, M.P.; Haick, H. Differentiation between genetic mutations of breast cancer by breath volatolomics. *Oncotarget* **2015**, *6*, 44864–44876. [[CrossRef](#)] [[PubMed](#)]
120. Mangler, M.; Freitag, C.; Lanowska, M.; Staech, O.; Schneider, A.; Speiser, D. Volatile Organic Compounds (VOCs) in Exhaled Breath of Patients with Breast Cancer in a Clinical Setting. *Ginekol. Pol.* **2012**, *83*, 730–736.
121. Phillips, M.; Cataneo, R.N.; Lebauer, C.; Mundada, M.; Saunders, C. Breath mass ion biomarkers of breast cancer. *J. Breath Res.* **2017**, *11*, 016004. [[CrossRef](#)]
122. Schmidt, K.; Podmore, I. Current Challenges in Volatile Organic Compounds Analysis as Potential Biomarkers of Cancer. *J. Biomarkers* **2015**, *2015*, 981458. [[CrossRef](#)]
123. Sun, X.; Shao, K.; Wang, T. Detection of volatile organic compounds (VOCs) from exhaled breath as noninvasive methods for cancer diagnosis. *Anal. Bioanal. Chem.* **2015**, *408*, 2759–2780. [[CrossRef](#)] [[PubMed](#)]
124. Silva, C.L.; Perestrelo, R.; Silva, P.; Tomás, H.; Câmara, J.S. Volatile metabolomic signature of human breast cancer cell lines. *Sci. Rep.* **2017**, *7*, srep43969. [[CrossRef](#)] [[PubMed](#)]
125. Tanaka, M.; Hsuan, C.; Oeki, M.; Shen, W.; Goda, A.; Tahara, Y.; Onodera, T.; Sanematsu, K.; Rikitake, T.; Oki, E.; et al. Identification of characteristic compounds of moderate volatility in breast cancer cell lines. *PLoS ONE* **2020**, *15*, e0235442. [[CrossRef](#)]
126. Cai, X.; Mai, R.-Z.; Zou, J.-J.; Zhang, H.-Y.; Zeng, X.-L.; Zheng, R.-R.; Wang, C.-Y. Analysis of aroma-active compounds in three sweet osmanthus (*Osmanthus fragrans*) cultivars by GC-olfactometry and GC-MS. *J. Zhejiang Univ. Sci. B* **2014**, *15*, 638–648. [[CrossRef](#)] [[PubMed](#)]
127. Yang, H.Y.; Wang, Y.C.; Peng, H.Y.; Huang, C.H. Breath Biopsy of Breast Cancer Using Sensor Array Signals and Machine Learning Analysis. *Sci. Rep.* **2021**, *11*, 1–9. [[CrossRef](#)] [[PubMed](#)]
128. Phillips, M.; Cataneo, R.N.; Ditkoff, B.A.; Fisher, P.; Greenberg, J.; Gunawardena, R.; Kwon, C.S.; Rahbari-Oskoui, F.; Wong, C. Volatile Markers of Breast Cancer in the Breath. *Breast J.* **2003**, *9*, 184–191. [[CrossRef](#)] [[PubMed](#)]
129. Phillips, M.; Cataneo, R.N.; Ditkoff, B.A.; Fisher, P.; Greenberg, J.; Gunawardena, R.; Kwon, C.S.; Tietje, O.; Wong, C. Prediction of breast cancer using volatile biomarkers in the breath. *Breast Cancer Res. Treat.* **2006**, *99*, 19–21. [[CrossRef](#)]
130. Wied, M.; Güntner, A.T.; Righettoni, M.; Pratsinis, S.E. P1DH.13—si-doped α -moo3 sensing nanoparticles for selective breath NH₃ detection. *Proc. IMCS* **2018**, *2018*, 681–682.
131. Li, H.-Y.; Huang, L.; Wang, X.-X.; Lee, C.-S.; Yoon, J.-W.; Zhou, J.; Guo, X.; Lee, J.-H. Molybdenum trioxide nanopaper as a dual gas sensor for detecting trimethylamine and hydrogen sulfide. *RSC Adv.* **2017**, *7*, 3680–3685. [[CrossRef](#)]

132. Yu, S.-Y.; Tung, T.-W.; Yang, H.-Y.; Chen, G.-Y.; Shih, C.-C.; Lee, Y.-C.; Chen, C.-C.; Zan, H.-W.; Meng, H.-F.; Lu, C.-J.; et al. A Versatile Method to Enhance the Operational Current of Air-Stable Organic Gas Sensor for Monitoring of Breath Ammonia in Hemodialysis Patients. *ACS Sensors* **2019**, *4*, 1023–1031. [[CrossRef](#)]
133. Le Maout, P.; Wojkiewicz, J.-L.; Redon, N.; Lahuec, C.; Seguin, F.; Dupont, L.; Mikhaylov, S.; Noskov, Y.; Ogurtsov, N.; Pud, A. Polyaniline nanocomposites based sensor array for breath ammonia analysis. Portable e-nose approach to non-invasive diagnosis of chronic kidney disease. *Sens. Actuators B Chem.* **2018**, *274*, 616–626. [[CrossRef](#)]
134. Ghosh, R.; Nayak, A.K.; Santra, S.; Pradhan, D.; Guha, P.K. Enhanced ammonia sensing at room temperature with reduced graphene oxide/tin oxide hybrid films. *RSC Adv.* **2015**, *5*, 50165–50173. [[CrossRef](#)]
135. Pathak, S.K.; Mishra; Gupta, B.D. Fiber optic ammonia sensing using Ag/SnO₂ thin films: Optimization of SnO₂ thin film thickness using electric field distribution and reaction factor. *Appl. Opt.* **2015**, *87*12, 29.
136. Maheswari, S.; Karunakaran, M.; Kasirajan, L.B.K. Ammonia sensors on the base of gadolinium doped tin oxide thin films and its characterization: Effect of doping concentration. *Phys. B Condens. Matter* **2021**, *602*, 412477. [[CrossRef](#)]
137. Rigoni, F.; Drera, G.; Pagliara, S.; Goldoni, A.; Sangaletti, L. High sensitivity, moisture selective, ammonia gas sensors based on single-walled carbon nanotubes functionalized with indium tin oxide nanoparticles. *Carbon* **2014**, *80*, 356–363. [[CrossRef](#)]
138. Feng, D.; Du, L.; Xing, X.; Wang, C.; Chen, J.; Zhu, Z. Highly sensitive and selective NiO/wo₃ composite na-noparticles in detecting H₂S biomarker of halitosis. *ACS Sens.* **2021**, *6*, 733–741. [[CrossRef](#)]
139. Hu, J.; Sun, Y.; Wang, X.; Chen, L.; Zhang, W.; Chen, Y. Synthesis and gas sensing properties of molybdenum oxide modified tungsten oxide microstructures for ppb-level hydrogen sulphide detection. *RSC Adv.* **2017**, *7*, 28542–28547. [[CrossRef](#)]
140. Choi, S.-J.; Lee, I.; Jang, B.-H.; Youn, D.-Y.; Ryu, W.-H.; Park, C.O.; Kim, I.-D. Selective Diagnosis of Diabetes Using Pt-Functionalized WO₃Hemitube Networks As a Sensing Layer of Acetone in Exhaled Breath. *Anal. Chem.* **2013**, *85*, 1792–1796. [[CrossRef](#)]
141. Shan, B.; Broza, Y.Y.; Li, W.; Wang, Y.; Wu, S.; Liu, Z.; Wang, J.; Gui, S.; Wang, L.; Zhang, Z.; et al. Multiplexed Nanomaterial-Based Sensor Array for Detection of COVID-19 in Exhaled Breath. *ACS Nano* **2020**, *14*, 12125–12132. [[CrossRef](#)]
142. Qiu, G.; Gai, Z.; Tao, Y.; Schmitt, J.; Kullak-Ublick, G.A.; Wang, J. Dual-functional plasmonic photothermal biosensors for highly accurate severe acute respiratory syndrome coronavirus 2 detection. *ACS Nano* **2020**, *14*, 5268–5277. [[CrossRef](#)]
143. Xia, S.; Luo, X. Analysis of 2D nanomaterial BC₃ for COVID-19 biomarker ethyl butyrate sensor. *J. Mater. Chem. B* **2021**, *9*, 9221–9229. [[CrossRef](#)] [[PubMed](#)]
144. Snitz, K.; Andelman-Gur, M.; Pinchover, L.; Weissgross, R.; Weissbrod, A.; Mishor, E.; Zoller, R.; Linetsky, V.; Medhanie, A.; Shushan, S.; et al. Proof of concept for real-time detection of SARS CoV-2 infection with an electronic nose. *PLoS ONE* **2021**, *16*, e0252121. [[CrossRef](#)] [[PubMed](#)]
145. Nurputra, D.K.; Kusumaatmaja, A.; Hakim, M.S.; Hidayat, S.N.; Julian, T.; Sumanto, B.; Mahendradhata, Y.; Saktiawati, A.M.I.; Wasisto, H.S.; Triyana, K. Fast and noninvasive electronic nose for sniffing out COVID-19 based on exhaled breath-print recognition. *NPJ Digit. Med.* **2022**, *5*, 115. [[CrossRef](#)] [[PubMed](#)]